Inter-room pollutant transmission routes in naturally ventilated street canyon buildings

Murtaza Mohammadi [a], John Kaiser Calautit [a,*], John S. Owen [b], Christof Gromke [c], Yupeng Wu [a], Hao Liu [a]

[a] *Department of Architecture and Built Environment, Faculty of Engineering, University of Nottingham, Nottingham, NG7 2RD, UK*
[b] *Department of Civil Engineering, Faculty of Engineering, University of Nottingham, Nottingham, NG7 2RD, UK*
[c] *Laboratory of Building and Environmental Aerodynamics, Institute for Hydromechanics, Karlsruhe Institute of Technology, 76128, Karlsruhe, Germany*

ABSTRACT

Airborne transmission of pollutants is a significant concern in urban areas, especially since the recent pandemic. While previous studies have explored inter-room pollutant crossflow in highrise buildings and isolated scenarios, the ventilation characteristics within street canyon configurations have not received enough attention. Understanding ventilation characteristics in this layout will help limit the spread of pollutants along the street. This study investigates the wind-driven transmission characteristics of pollutants between the indoor rooms situated adjacent to a street canyon, subjected to perpendicular approach flow. Numerical simulations were performed using the 3D steady Reynolds-Averaged Navier-Stokes approach and validated against surface pressure measurements inside a wind tunnel. The impacts of seven building ventilation strategies were compared, each representing a window opening combination on the two buildings. Based on the set environmental conditions, the results indicate that the inter-room transmission is dependent on both the ventilation efficiency and the specific location of the room. Increasing the ventilation rate decreases the cross transmission between the rooms, while rooms at the centre of the canyon have an increased susceptibility of being contaminated. For instance, switching from cross to single-sided ventilation decreased the average air change rate from $42.3h^{-1}$ to $1.4h^{-1}$, coinciding with a rise in pollutant concentration by 114-fold and 12-fold at the canyon's centre and side, respectively. Rooms at the edge of the canyon were more contagious and could contaminate other rooms located further inside the street, albeit in small doses. Our findings present new insights within the domain of indoor-outdoor air interaction, shedding light on the interplay between room location and potential inter-unit pollutant transmission. In addition, the pressure measurement results from the wind tunnel experiment provide a valuable resource for other researchers aiming to validate numerical simulations for building engineering applications.

1. Introduction

Air quality plays an important role in affecting the health and mortality rate of a population. The Global Burden of Disease [1] attributed about 6.67 million deaths in 2019 to air pollution alone, accounting for about 11–12% of all annual deaths. The huge

economic and wellbeing impacts of polluted air have been a matter of policy discussions and urban management goals, including the Sustainable Development Goals (SDG) [2]. It has been argued that air quality should be treated as a fundamental right of individuals [3]. Epidemiological studies have repeatedly emphasised its importance and the need to find solutions for a better quality of life and longer life expectancy [4–6]. A range of air pollutants, including CO, NOx, SOx, etc., can induce primary and secondary health impairments in humans and animals [7,8], as well as exacerbate underlying medical conditions [9–11]. Therefore, buildings and indoor spaces should be designed to limit pollution and pathogen levels, for a safe and healthy environment.

In urban areas, pollutants can spread between different indoor rooms (or units) and pose significant health risks. Several epidemiological studies have highlighted the airborne transmission of pathogens between apartments which has led to the spread of diseases [12–14]. Similarly, indoor generated air pollutants from activities such as cooking, heating, mechanical equipment, smoking, construction, etc. [15–17], can be transported to other units through airborne routes. In the case of naturally ventilated spaces, the risks can be higher if the incoming air is not filtered. While the nature of infection can vary depending on the microorganism and dosage, it is important to understand the pathways of transmission to limit the inter-unit spread of pathogens as well as other pollutants.

Considering the associated risks from inter-unit cross-transmission, several studies have been conducted to identify possible pathways in buildings and design suitable interventions. Mu et al. [18–20] conducted a series of wind tunnel tests to identify the role of wind direction and source location on the inter-unit transmission for an isolated highrise building. Similarly, Liu et al. [21] conducted a decoupled simulation to estimate the risks of cross-transmission in an isolated highrise building. Their results demonstrated that a windward-located pollutant source can intensify the pollution concentrations in adjacent flats. Wang et al. [22] performed simulations to understand the role of window type on the cross-transmission of pollutants in an isolated building and showed that an awning window offers the most protection against the transmission of contaminants. More recently, Huang et al. [23], developed a numerical model to estimate the cross-transmission risk in highrise buildings by measuring the concentrations of a tracer gas in an outdoor environment. Several other studies have explored the effect of building geometry and grouping to assess inter-unit transmission [24–29]. However, most work in this domain has been limited to the assessment of highrise buildings. In contrast, studies on cross-transmission of pollutants in street canyons, representing an important and ubiquitous urban feature, remain few.

Generally, studies on pollution transmission in street canyons have been limited to outdoor pollution dispersion [30–39] or transmission of outdoor air pollutants into indoor spaces [40–44]. A few studies on inter-unit transmission in street canyons have been conducted in the last couple of years. Dai et al. [45,46] conducted field experiments, using a scaled model of a street canyon, to study the effect of wind and temperature on inter-unit transmission. Rows of concrete blocks were placed to form street canyons, and several model buildings with indoor units placed at the centre of the streets. By measuring the tracer gas concentrations, they observed that the concentration of transmitted pollutants was inversely related to the air change rate (ACH). Transmission primarily occurred in vertically downward direction from sources on the windward façade. Likewise, transmission from leeward façade was vertically upward. The authors associated this to the presence of a stable vortex inside the street canyon. The transmission across the street canyon into rooms located on the opposite buildings was much lower, although at some instances they observed a spike in the pollutant concentration. In fact, they found that the re-entry ratio was higher for a room located further downwind than in the immediate vicinity. While the study makes some important contribution in the field of inter-unit dispersion, a generalised conclusion is difficult to draw and is not easily replicable due to transient nature of the outdoor meteorology. A wind tunnel investigation by Cui et al. [47] attempted to understand the dispersion characteristics of hot smoke released from the mid-height of a building adjacent to a street canyon. They highlighted that wind speed, buoyancy and height of the source unit are critical factors which determine whether the released pollutants will recirculate inside the canyon or get washed downwind. They concluded that the released pollutant was primarily transmitted vertically upwards when released on the windward façade, contrary to the observations by Dai et al. [46]. Finally, a recent work by Zheng et al. [48] explores the effect of ventilation strategies in hospital dormitories on the inter-unit transmission of pathogens. The work briefly discusses the effect of aspect ratio of street canyon on dispersion of pathogens. However, further work is warranted to understand the role of ventilation in street canyons and the inter-unit transmission routes.

With the advent of improved computational facilities, several studies on the ventilation of indoor spaces have been conducted [41, 49,50]. However, one of the major challenges with numerical tools is their reliability and replicability, as they need to be validated against experimental observations. In numerous instances, researchers have adopted a mixed-validation strategy wherein the model being studied has geometric and spatial distinctions from the validation model assessed experimentally [20,51–55]. For example, Yang et al. [50] and Wang et al. [56] simulated multistorey buildings integrated with indoor units, and validated their models using the WT tests conducted by Jiang et al. [57], - which analysed air flow inside an isolated cube. Wu and Niu [58] simulated an isolated multistorey building with indoor units but validated their model using experimental results by Perino and Heiselberg [59], which measured airflow and ventilation inside a chamber. Similarly, Ai and Mak [60] validated their multistorey urban canyon model with indoor units against experimental results by Dascalaki et al. [61] which measured airflow and ventilation rate inside a chamber. While the authors made efforts to ensure accuracy in their results, it should be noted that the simulation domain under investigation differs significantly from the experimental model, potentially altering the physics of the airflow. Therefore, it is possible that the numerical results do not accurately reflect the real flow characteristics.

Noting the scarcity of literature on cross-contamination of indoor spaces adjacent to street canyons, this study aims to provide a comprehensive assessment of the effect of natural ventilation mode on indoor air quality and transmission. A CFD model is developed using Ansys FLUENT ® and validated against two wind tunnel tests: (i) building internal pressure (conducted as part of this study) and (ii) outdoor street canyon pollutant dispersion (obtained from literature). The model was used to simulate various window opening strategies on two parallel buildings forming a street canyon subjected to a perpendicular approach flow. Instead of relying on outdoor measurements to estimate indoor pollution levels, the current study adopts a coupled approach by integrating both indoor and outdoor domains and introducing a source of pollutant inside each individual room. This will help understand the dispersion and airborne

routes for inter-unit contamination along street canyons and identify critical scenarios. The novelty of the present work is as follows:

- A 1:100 scale model of the street canyon integrated with indoor units is built and tested inside an atmospheric boundary layer (ABL) wind tunnel to understand dominant indoor pressure trends. The results can be used by other researchers to validate their numerical model.
- A 3D CFD model is developed and validated to understand transmission routes from one apartment (unit) to other apartments along the length and height of the street. The building is compartmentalised into rooms on three different floors.

2. Methodology

2.1. Wind tunnel setup for indoor airflow

A series of experiments were conducted inside an atmospheric boundary layer wind tunnel at the Department of Civil Engineering, University of Nottingham, to measure the air pressure inside an indoor space adjacent to a street canyon. The test section is 2.4 m wide by 1.8 m high and has a fetch of 11.5 m to the front of a 2 m diameter circular turntable. The experimental model is based on the earlier works by Gromke et al. [62] and Cui et al. [47]. A combination of fence and spires at the inlet, along with cuboidal roughness elements along the fetch, is used to generate the required ABL profile. An image of the canyon model and the test section is shown in Fig. 1, along with the wind profile measured at the centre of the empty turntable.

A reduced-scale model of the street canyon, with a ratio of 1:100, was placed on the turntable, perpendicular to the wind direction. The 1.2 m long model street canyon was formed by two parallel building blocks of height H = 120 mm and depth B = 120 mm. The model blocks were placed apart creating a street of width W = 120 mm. A three-storey indoor domain was made of 2 mm thick transparent sheets and placed at the centre of each of the blocks. Internal dimensions of the rooms measured H × W × D = 37 mm × 62 mm × 116 mm, with a 12 mm square window cut on the external faces of the room. In order to assess internal pressure levels, 15 pressure taps were placed across the internal wall of each room, and evenly arranged in a grid of 20 mm horizontal and 9.5 mm vertical. Vinyl tubes were used to connect the taps to a pressure transducer, a Scannivalve MPS4264, capable of measuring up to 995.4
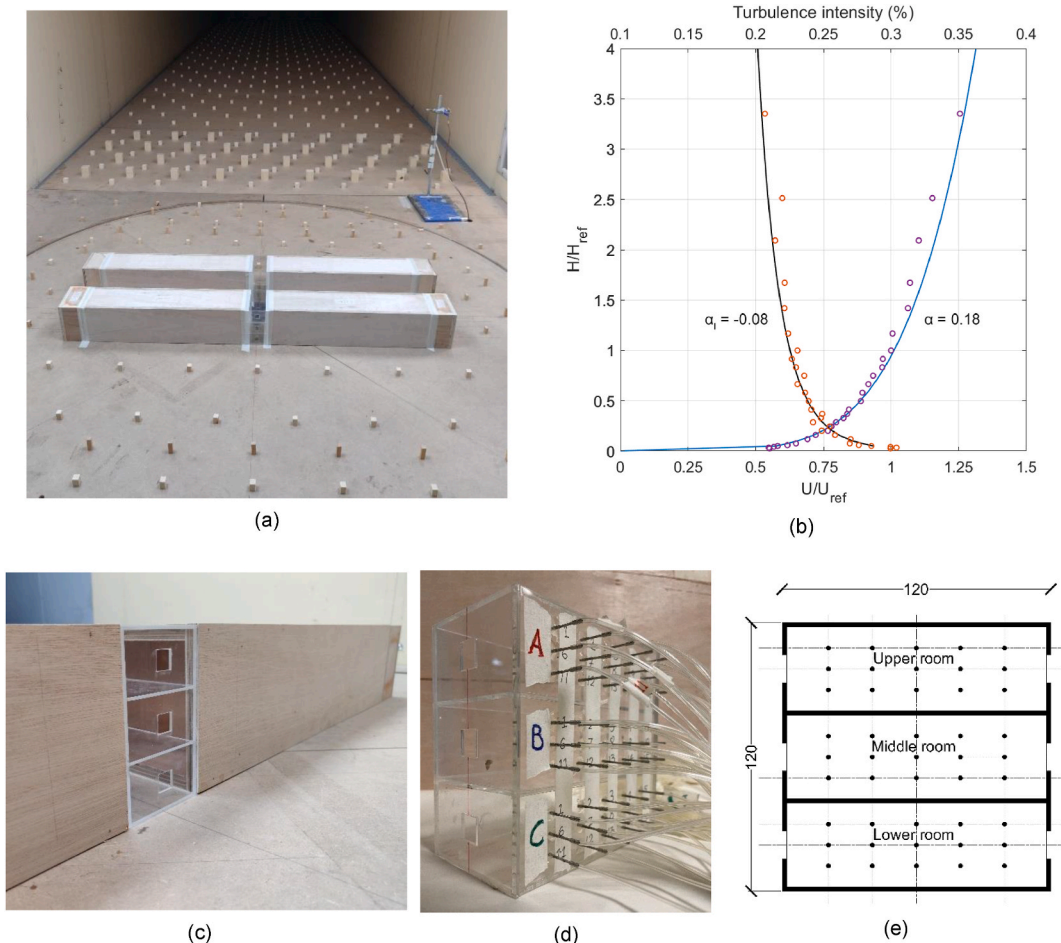

Fig. 1. (a) The canyon model placed on the turntable with roughness elements; (b) Wind profile in the empty test section; (c) Close-up view of the indoor domain with three floors; (d) Pressure tubes connected to a side wall of the indoor domain; (e) Location of pressure taps inside the rooms.
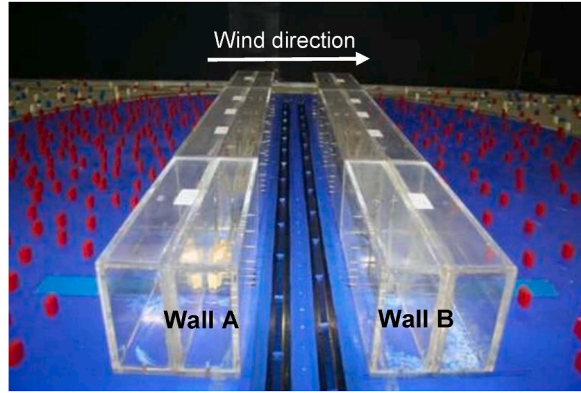
Fig. 2. The experimental setup for pollutant dispersion in a street canyon, image courtesy [63].

Pa at $\pm0.2\%$ accuracy. The reference pressure was measured by placing a pitot-static tube 1.1 m upstream of the model.

2.2. Wind tunnel setup for pollutant dispersion

The experimental data for pollutant dispersion in the outdoor domain of street canyons was accessed from the CODASC database [63]. The physical dimensions of the scaled street canyon model are the same as described in the previous section. However, no indoor rooms were placed in this experiment and only the outdoor dispersion of a tracer gas was analysed. Four line-sources of pollutants were introduced in the canyon at the street level and a tracer gas was released from them. The mean outdoor concentrations of the tracer gas were measured at the canyon walls and normalised according to Eqn. (1) for line-source emission [64].

$$C^+ = \frac{C u_{ref} H}{Q/l} \tag{1}$$

where C is the measured mean concentration, u_{ref} is the wind speed at reference height H and Q/l represents the emission strength per unit length of the source. Fig. 2 shows the experimental setup at the Karlsruhe Institute of Technology and more information about same is available online [63].

2.3. Numerical setup

2.3.1. Computational domain and boundary conditions

The CFD model of the street canyon consists of two parallel building blocks, each of length L = 120 m and depth of B = 12 m, separated by a road of equal width, i.e., W = 12 m. The buildings are three storeys high, with a total height of H = 12 m, thus achieving an aspect ratio of unity (H/W = 1). The domain size was set based on the recommendations by COST Action C14 [65], summarised in Fig. 3. An inner domain with a refined grid was created around the canyon with dimensions 18H, 3H and 5H in width, height, and depth, respectively, following Salim et al. [66]. This is done to ensure a more reliable prediction of flow variables with large gradients within the region of interest.

The computational mesh consisted of hexahedral elements mostly, with the smallest elements located inside the indoor space, measuring $\delta x = \delta y = \delta z = 0.01H$. The discretisation scheme ensured that at least 10 cells were generated across the length of any edge, as suggested by Franke et al. [65]. The mesh consisted of 6.4 million cells after mesh sensitivity analysis. It was found that any further refinement beyond this did not produce any detectable improvement in the results. Instead, it led to higher computational demand and therefore, subsequent research was carried out using this mesh setting. Details of the mesh sensitivity analysis are presented in Appendix A. The inlet wind profile was identical for all simulation test cases. The mean wind speed was based on the fitted power law curve from the WT measurement (section 2.1) and is given by Eqn. (2). The turbulent kinetic energy and the dissipation rate were calculated using Eqns. (3) and (4), respectively.

$$u(z) = u_{ref} \left(\frac{z}{z_{ref}} \right)^{\alpha} \tag{2}$$

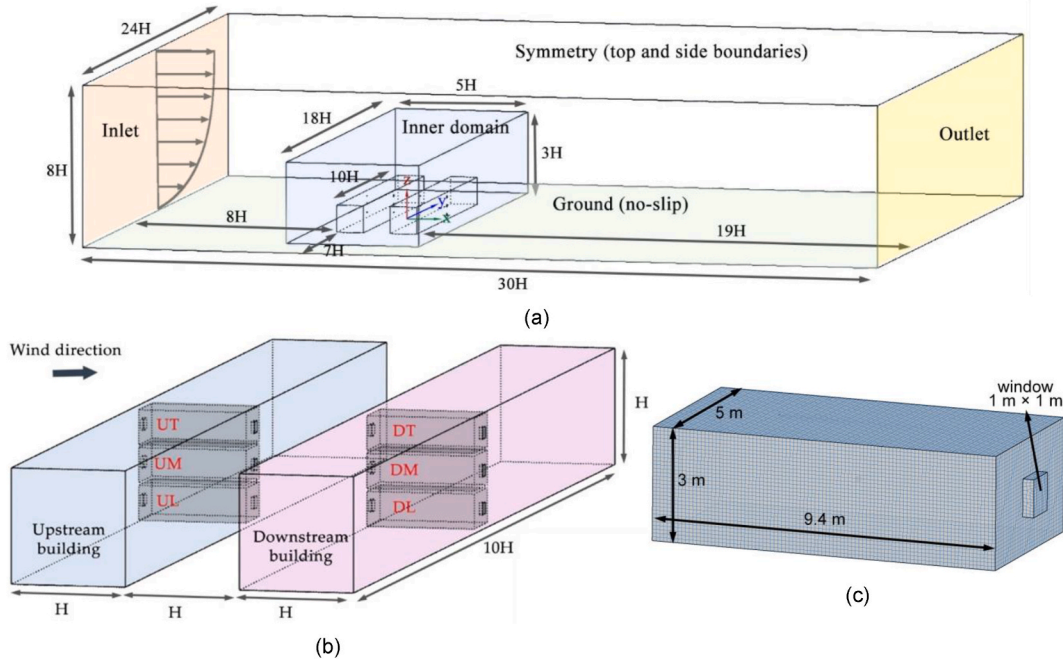$$k(z) = \frac{3}{2} (u(z) \times I(z))^2 \tag{3}$$

Fig. 3. Model configuration; (a) Domain size and boundary conditions, (b) Building configuration and location of indoor rooms, (c) Size of indoor room and with surface mesh.

$$\varepsilon(z) = C_\mu^{3/4} \frac{k(z)^{3/2}}{l} \tag{4}$$

where the reference velocity $u_{ref} = 4.6$ m/s, the reference height $z_{ref} = H$, α is the power law exponent found by curve fitting the wind tunnel data (see Fig. 1(b)) and the empirical constant $C_\mu = 0.09$. The streamwise turbulence intensity, I, is the ratio of the standard deviation of the measured velocity to the mean wind velocity. Since the model canyon is a low-rise long building configuration, the contribution of wind-driven air flow is much more significant than other factors [67], and consequently, isothermal conditions were assumed in order to study inter-unit dispersion of pollutants.

2.3.2. Turbulence model and emission source

Turbulent flows with fluctuating velocity fields characterise airflow in urban areas. While the Reynolds-averaged Navier-Stokes (RANS) closure models govern the transport of the averaged flow quantities by modelling the entire range of turbulence scale [68], Large Eddy Simulation (LES) equations explicitly compute the large eddies. Thus, predictions of flow features are more accurate, including dispersion characteristics of pollutants [69]. However, LES requires more computational resources and developing sub-grid-scale models is a challenge, including the specification of time-dependent boundary conditions [70]. Nevertheless, RANS models, including the Reynolds Stress Model (RSM), have been extensively used in previous studies and validated to predict the dispersion of pollutants in 2D as well as 3D urban canyons [62,71–73]. Since the aim of this study was to understand the impact of ventilation choice on the bulk crossflow of pollutants between the various indoor units (or rooms), a knowledge of average pollutant exposure values within a space can provide sufficient information for appraisal. The performance of four different steady-state RANS models was tested, namely the standard k–ε, RNG k–ε, standard k–ω and the RSM turbulence model. The validation of the CFD model revealed the superior performance of the RSM model (section 2.4), hence the assessment of inter-unit dispersion was carried out with the RSM model.

Indoor pollutant concentration was estimated by solving the transport equations for passive tracer gas released at a constant rate of 0.182×10^{-6} kg/s from point sources at the centre of the rooms. The dispersion of the pollutant was based on the standard steady-state advective-diffusion model, where the turbulent Schmidt number (Sc_t) determines the diffusivity. A range of Sc_t values from 0.2 to 0.9 were tested to evaluate the performance, before $Sc_t = 0.3$ was selected [44,74–76]. The transmitted pollutant concentration values were then normalised with respect to the source strength, reference height and velocity, given by Eqn. (5) for point-source emission [77].

$$K = \frac{C u_{ref} H^2}{Q} \tag{5}$$

where C is the average mass concentration of a tracer gas (kg/m^3) in the room, Q is the emission rate of the tracer gas and u_{ref} is the reference velocity at the building height H. The SIMPLE scheme was used for pressure-velocity coupling in conjunction with the

second-order upwind scheme to discretise the convective and diffusion terms. The enhanced wall function was used for the near-wall treatment [76,78–81].

2.4. Validation

2.4.1. Validation of internal room flow and pressure field

The results from the wind tunnel measurement and CFD simulations were analysed in terms of pressure coefficient (C_p), given by Eqn. 6

$$C_p = \frac{p - p_{ref}}{0.5\rho u_{ref}}$$ (6)

Where p is the measured pressure, p_{ref} is the reference pressure and ρ is the air density. The average C_p values along the rooms' internal walls are presented in Table 1. There is under-pressure in all the rooms, indicated by the negative C_p. When both windows are open, the flow resembles a jet through the room from window to window. This jet entrains air at its surroundings and consequently, a suction is established in the room (contour plots of C_p are presented in Appendix B). However, the magnitude of the negative C_p varies between the upstream and downstream rooms, with a higher negative C_p in the downstream room, possibly due to the sheltering effect of the upstream building. WT observations indicate C_p in the range of [-0.56 to -0.60] for the downstream rooms and C_p in the range of [-0.25 to -0.26] for the upstream rooms. The downstream C_p predictions by the CFD models are more or less uniform across the three rooms, although the values are generally overpredicted in comparison to the WT observation. The overall difference across the rooms is the least for the RSM model. In the case of the upstream rooms, all four turbulence models overpredict the surface pressure on the top rooms (UT). The standard k-ε model fairly replicates the internal surface pressure in rooms UL and UM. In contrast, the prediction by the RSM model only closely matches the top room UT.

After undertaking a meticulous scrutiny of the flow patterns in the upstream room (across a vertical plane), it was observed that the streamwise flow patterns predicted by the RSM were similar to those of other turbulence models. Specifically, an upward jet flow pattern was identified immediately after the inflowing air entered the window opening, propelling the flow towards the ceiling. Additionally, a recirculation zone was detected in the lower section of the room, which was observed across all turbulence models, including the RSM. This shows that the RSM performs similar to the other turbulence models in simulating internal air flow. One plausible explanation for the observed divergence in the C_p values for rooms UL and UM could be attributed to the orientation of the inflowing air in the spanwise direction. Depending on the turbulence model used, the jet flow could be directed more prominently towards one side of the room, thus substantially affecting the C_p values, particularly in light of the fact that the measurements were taken on only one side of the room during the experiment. Additionally, airflow near the upstream building is highly 3-dimensional characterised by impinging, separation and vortex shedding [82], making it difficult to predict precisely.

A validation metric was developed to further assess the quality of the simulations. The COST Action 732 [83] document describes some of the performance indicators that can be used to validate a numerical simulation. Namely, the correlation coefficient (R), the normalised mean squared error (NMSE), the fractional bias (FB), the fraction of predictions within a factor of two of the observations (FAC2) and the hit rate (HR) were deemed appropriate for this study. They have been calculated (for all 45 measurement points) and summarised in Table 2 for the different turbulence models.

In terms of R and FAC2, all models meet the acceptance criteria, suggesting that the deviations in C_p values are within reasonable limits and that the general trend is as observed in the WT. For the NMSE and FB metrics, which puts more stress on the higher prediction values, the RNG k-ε and standard k-ω models did not meet the acceptance threshold. Meeting NMSE criteria ensures that

Table 1

Comparison of internal wall room average pressure coefficient between WT and CFD data, mean and standard deviation (in brackets).

Turbulence model	Upstream rooms			Downstream rooms		
	UL	UM	UT	DL	DM	DT
Wind tunnel	-0.25 (0.016)	-0.25 (0.019)	-0.26 (0.022)	-0.58 (0.011)	-0.60 (0.009)	-0.56 (0.014)
Standard k-ε	-0.20 (0.018)	-0.23 (0.016)	-0.40 (0.012)	-0.73 (0.003)	-0.75 (0.003)	-0.74 (0.002)
RNG k-ε	-0.33 (0.012)	-0.25 (0.021)	-0.41 (0.014)	-0.78 (0.005)	-0.79 (0.004)	-0.85 (0.007)
Standard k-ω	-0.33 (0.014)	-0.28 (0.022)	-0.38 (0.008)	-0.81 (0.006)	-0.89 (0.006)	-0.87 (0.006)
RSM	-0.07 (0.021)	-0.06 (0.016)	-0.31 (0.012)	-0.64 (0.008)	-0.67 (0.007)	-0.68 (0.005)

Table 2

Validation metrics for the internal pressure coefficient.

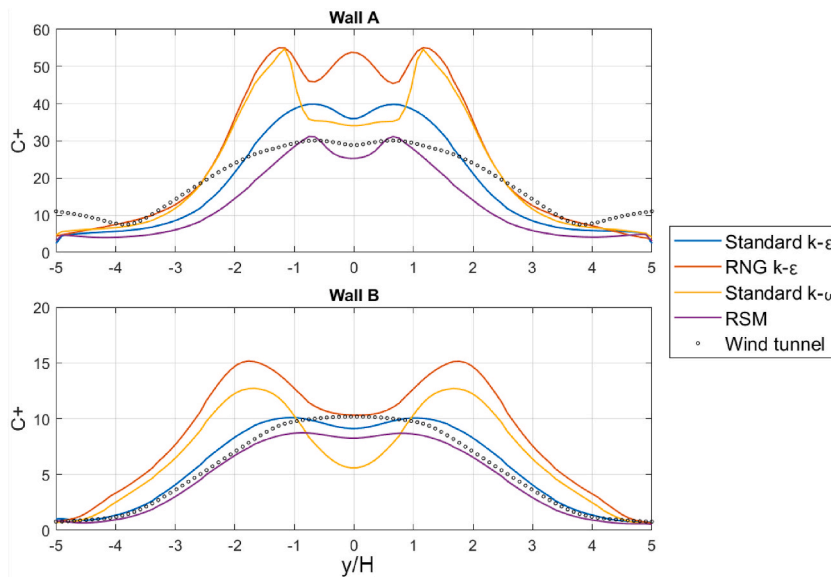| Model	R	NMSE	FB	FAC2	HR
Standard k-ε	0.969	0.077	-0.200	1	0.46
RNG k-ε	0.975	0.130	-0.307	1	0.22
Standard k-ω	0.989	0.165	-0.342	1	0.28
RSM	0.957	0.088	0.033	0.67	0.64
Target	1	0	0	1	1
Acceptance criteria	>0.8	<1.5	[-0.3, 0.3]	>0.3	>0.6

Fig. 4. Comparison of normalised concentration C^+ extracted along the walls at z/H = 0.5.

random scatters are limited. Lastly, the HR was calculated with an absolute difference of 0.25 and a relative difference of 0.08, as indicated in the VDI guidelines [64]. It can be clearly seen that only the RSM model meets the acceptance threshold for this metric, which basically assesses the fitness of the model for the investigated purpose [84], i.e., airflow through the indoor domain adjacent to a street canyon. While the RSM turbulence model deviates from the WT observation in the rooms UL and UM (Table 1), the overall metric in Table 2, calculated across both upstream and downstream rooms, outperforms over the other turbulence models.

While there remains scope for further improvement in the accuracy of the CFD simulations, the current model performs satisfactorily well and can replicate WT observation at sufficient accuracy. Additional assessments of the numerical model should encompass validating the airflow patterns and air exchange within the room. It is imperative to acknowledge that despite the availability of hot wire anemometers to facilitate the measurement process, the dimensions of the model room proved too small to accommodate the hot wire sensor without causing interference to the airstream. As such, further experimentation is warranted to validate the numerical modelling, perhaps by employing optical measurement techniques. In the case of the downstream rooms, the RSM model provided the most accurate C_p prediction across the three rooms. The result is consistent with the literature [62,85,86], which has demonstrated that the RSM is particularly suited for complex flows exhibiting strong anisotropy and recirculation regions.

2.4.2. Validation of outdoor wind flow and pollutant dispersion

For this assessment, the boundary condition imposed in the CFD was based on the CODASC experiment data set and the normalised pollutant concentration (C^+) values were calculated according to Eqn. (1) (for line-source). Fig. 4 shows the C^+ values extracted along the mid-height of the canyon-facing walls – A (leeward) and B (windward). The x-axis represents the normalised distance along the canyon, normalised with respect to the street length, where the centre of the canyon is at y/H = 0. The distribution indicates higher C^+ values on wall A as compared to wall B, accompanied by higher pollutant concentration near the centre of the canyon. The predictions by RNG k-ε and standard k-ω are generally higher than WT observations on both walls A and B, especially in the region y/H = [-2 to -1] ∪ [1 to 2] on wall A. In fact, the RNG k-ε model consistently overpredicts the pollutant concentration throughout the length of the canyon, except at the canyon ends. Contrastingly, the standard k-ε and RSM model are able to reasonably reproduce the WT observation, with the performance of RSM being better on wall A. In general, the RSM model closely captures the experimental observation, with higher concentrations in the range of C^+ = [0 to 40] on wall A and a lowered concentrations up to C^+ = 10 on wall B.

Contours of C^+ values are shown in Fig. 5 to further illustrate the pollutant distribution pattern for the WT study and RSM model. It
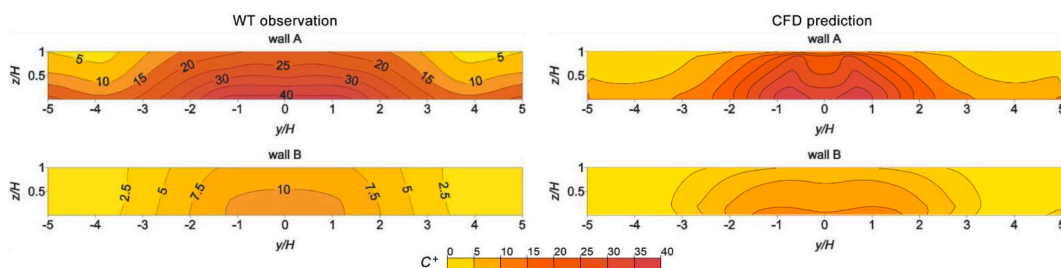

Fig. 5. Comparison of normalised concentration C^+ between the experiment [63] and the current RSM turbulence model.

Table 3
Validation metrics for the normalised pollutant concentration at the walls.

Model	R	NMSE	FB	FAC2	HR
Standard k-ε	0.949	0.121	-0.008	0.97	0.63
RNG k-ε	0.943	0.475	-0.369	0.71	0.32
Standard k-ω	0.929	0.294	-0.217	0.93	0.38
RSM	0.936	0.189	0.294	0.78	0.59
Target	1	0	0	1	1
Acceptance criteria	>0.8	<1.5	[-0.3, 0.3]	>0.3	>0.6

is evident that the overall dispersion of pollutants is similar between the WT and CFD results, despite a few deviations. Notably, the CFD predictions show a slight drop in C^+ at the centre of the canyon, forming a local minimum. Similarly, CFD simulation under-predicts the concentration values near the edges of wall A. This is possibly because the computational model is unable to accurately replicate the interaction between the canyon vortex (with a horizontal axis) and the edge vortex (with a vertical axis) near the building corners. Pollutant dispersion near $y/H = \pm 5$ is more strongly governed by the edge vortex, developed as a result of separation around the leading corner of the upstream building.

Simulation performance indicators, as described in the previous section, were calculated and are summarised in Table 3. Of the four turbulence models tested, all meet the acceptance criteria for correlation coefficient (R), NMSE, and FAC2. This suggests that the simulations can fairly replicate the outdoor flow field and dispersion characteristics, with limited random scatter. All of the turbulence models, except for RNG k-ε, meet the acceptance standards for FB. In terms of HR, the standard k-ε model meets the acceptance criteria while the RSM model nearly meets the acceptance threshold. Dispersion being turbulent in nature, predicting precise values is often challenging, leading to spatial variability [87]. Nevertheless, the deviations were considered acceptable since the focus of the research was more towards indoor air quality and the effect of ventilation. We also compared the velocity prediction inside the canyon to assist us in the validation process (see appendix B, Fig. B2). Agreeably, the performance of RSM and standard k-ε was quite close [76], but the choice of RSM was substantiated as the predictions within the region of interest were most close to the experimental data, and the results from both validation studies demonstrated the superior performance of RSM. Therefore, the RSM model was implemented for assessing the seven ventilation cases.

2.5. Simulation test cases and ventilation efficiency estimation

To evaluate inter-unit transmission in street canyons, we created a model of internal units (or rooms) within the buildings, at three specific locations along the canyon: the centre and the edges. These locations were based on the results of earlier works, notably [30, 62], which demonstrated that pollutant concentration is highest near the centre of the canyon and least near the edges, when the wind direction is perpendicular. Likewise, we created models of three-storey internal rooms located at the centre and edges of the street canyon. Fig. 6 shows the location of the rooms and the names assigned to them.
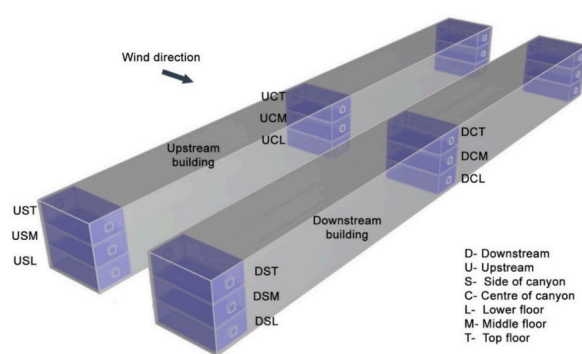
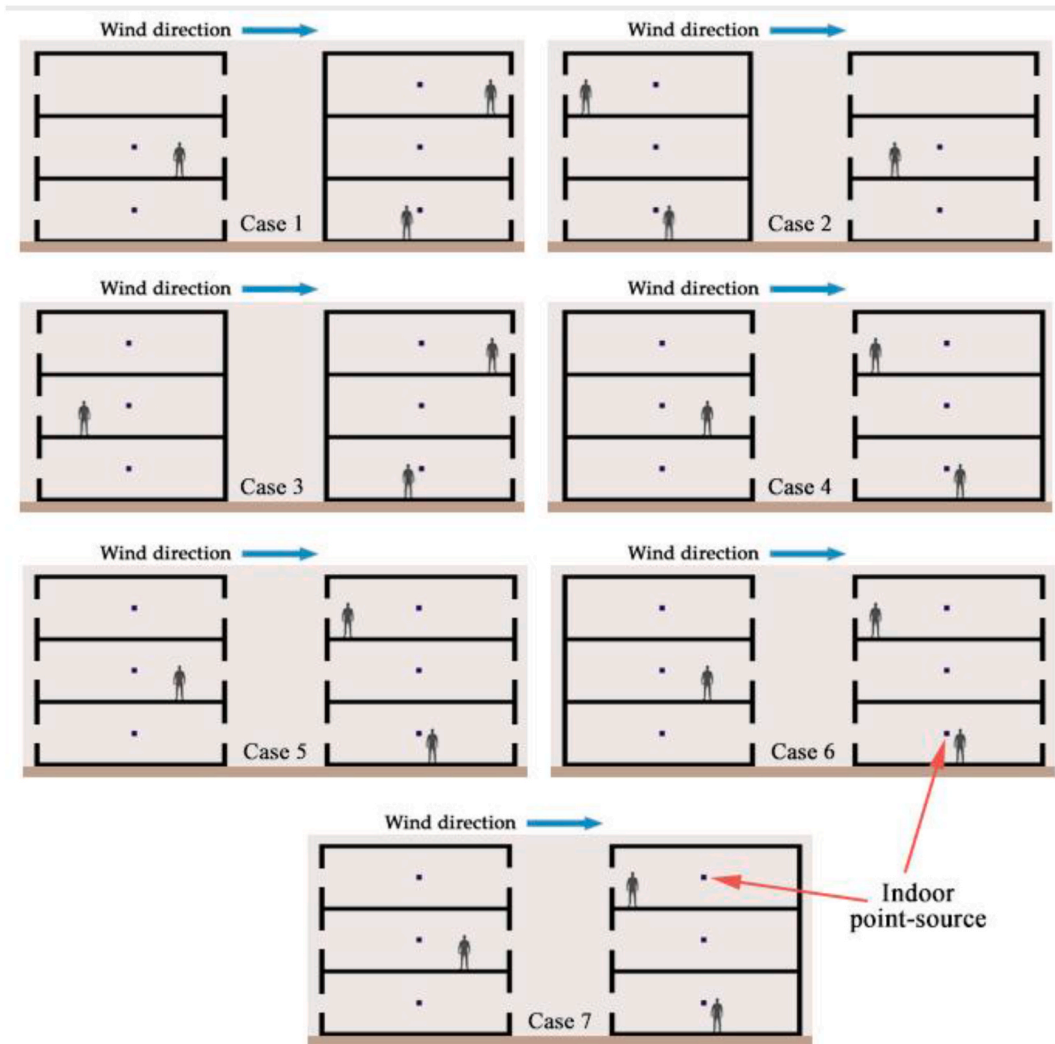**Fig. 6.** The simulated street canyon with internal rooms.

Fig. 7. Ventilation modes simulated in this study.

Seven building ventilation scenarios involving a mixture of single-sided and cross-ventilation were investigated in this study. In each case, all rooms of a building were assigned the same window opening strategy. Fig. 7 describes the window opening strategy for each of the ventilation cases. In case 1, the upstream building is cross-ventilated, whereas the downstream building is ventilated from the leeward side. In case 2, the upstream building is ventilated from the windward side, and the downstream building is cross-ventilated. Cases 3 and 4 represent only single-sided ventilation, one away from the street and the other from the street, respectively. In case 5, both buildings are cross-ventilated. In cases 6 and 7 one building is cross-ventilated while the other is ventilated form the street. The tracer gas, ethane, was released from a point source located at the centre of the room, at a height of 1.5 m, representing average indoor emissions.

While there are multiple combinations of window opening strategies on the façade of a building, simulating all of them is nearly impossible due to high computational demand. We have, therefore, studied seven relevant combinations of ventilation strategies, with a special focus on configurations expected to exhibit extreme pollutant concentration. The study of these selected configurations provides valuable insights into the general transmission characteristics and can inform the development of more advanced computational models for predicting indoor air quality in real-world buildings. Therefore, while the current study is limited in the number of ventilation scenarios, the approach provides a basis for future research in the domain.

There are various indices to measure the ventilation efficiency of a room, including air change rate per hour (ACH) [88], age of air [89] and air exchange efficiency [90]. The measure of the net flow of air required to remove all pollutants from a space is known as the purging flow rate (PFR), and it is an essential indicator for evaluating the ventilation efficiency of a local domain [91], such as the indoor rooms studied here. The PFR can also be understood as the equivalent rate at which fresh air is supplied to the domain [92]. For this work, the ACH calculated by PFR is used as it offers a better comparison of ventilation efficiency between the simulated rooms [50]. It is calculated by Eqn. (7);

$$ACH_{PFR} = \frac{3600 * \frac{Q}{V}}{\int_0^V C \, dV} \tag{7}$$

where Q is the emission strength of 0.182×10^{-6} kg/s and is constant for all emission sources, C is the mass concentration of the tracer gas and V is the volume of the room.

3. Results and discussion

The results from the simulation were analysed based on two parameters: the normalised concentration of adventitious pollutants in a room and the ventilation efficiency of that room. The findings are presented in a tabular format, which shows the cross-transmitted pollutant between each pair of rooms. The columns represent the pollutant source while the rows indicate the target room. The pollutant concentration values were normalised using Eqn. (5). Since, the transmission from rooms at one end of the canyon to the rooms at the other end was negligible ($K < 10^{-10}$), they have not been included in the discussion. Additionally, both sets of side (or corner) rooms played, due to symmetric conditions, an equal role towards the contamination of central rooms, which allowed analysis of one set of corner rooms alone (DSL, UST etc., see Fig. 6).

3.1. Ventilation case 1

Table 4 shows the cross-transmitted pollutants between each pair of rooms for the ventilation case 1. In this mode, the upstream building is cross-ventilated, and the downstream building is ventilated from the leeward side. Pollutants are primarily accumulated in the downstream rooms, with contributions from all surrounding rooms. Vertical transmission of pollutants from the lower to upper rooms in the downstream building is the most critical route. The room DCM is severely contaminated with pollutants from DCL ($K = 49.99$), whereas DCT is majorly contaminated with pollutants from DCM ($K = 43$). A similar observation is made for the rooms at the side of the canyon (DSL, DSM and DST), but with lowered concentration values ($K = 11.57$ and 9.19, respectively). In contrast, cross-ventilation in the upstream building produces negligible inter-unit transmission ($K < 0.01$).

The rooms on the upstream building are also accompanied by high ACH_{PFR}, in the range of 40 h^{-1} to 80 h^{-1}, while the downstream building is poorly ventilated with $ACH_{PFR} \approx 1$ h^{-1}. However, it is important to note that the upstream rooms still contribute to the pollution levels in the downstream rooms, even if the inter-unit transmission is limited between them. Transmission from upstream to downstream rooms is more pronounced across-the-street as against along-the-street. This is illustrated in Table 4, where the deeper shade of yellow for across-the-street transmission of pollutants contrasts with the lighter shade for along-the-street transmission, with a difference in K value by two orders of magnitude. A further examination reveals that the strength of transmission from the side rooms on the upstream building (USL, USM and UST) is twice that of the central rooms (UCL, UCM and UCT).

Table 4
Normalised pollutant concentrations (K) in case 1.

Source / Target		Upstream						Downstream						ACH_{PFR} (h^{-1})
		USL	USM	UST	UCL	UCM	UCT	DSL	DSM	DST	DCL	DCM	DCT	
Upstream	USL		0.00	0.00	0.00	0.00	0.00	0.00	0.00	0.00	0.00	0.00	0.00	38.4
	USM	0.00		0.00	0.00	0.00	0.00	0.00	0.00	0.00	0.00	0.00	0.00	46.2
	UST	0.00	0.00		0.00	0.00	0.00	0.00	0.00	0.00	0.00	0.00	0.00	49.9
	UCL	0.00	0.00	0.00		0.00	0.00	0.00	0.00	0.00	0.00	0.00	0.00	82.5
	UCM	0.00	0.00	0.00	0.00		0.00	0.00	0.00	0.00	0.00	0.00	0.00	75.3
	UCT	0.00	0.00	0.00	0.00	0.00		0.00	0.00	0.00	0.00	0.00	0.00	68.2
Downstream	DSL	0.46	0.49	0.46	0.02	0.02	0.02		2.59	0.32	0.05	0.03	0.02	0.5
	DSM	0.45	0.48	0.45	0.02	0.02	0.02	11.57		0.43	0.05	0.03	0.02	0.7
	DST	0.44	0.46	0.44	0.02	0.02	0.02	4.25	9.19		0.06	0.03	0.02	0.8
	DCL	0.06	0.06	0.06	0.21	0.22	0.24	0.15	0.10	0.03		0.89	0.51	1.0
	DCM	0.05	0.06	0.06	0.23	0.24	0.27	0.15	0.09	0.03	49.99		1.15	1.2
	DCT	0.05	0.05	0.05	0.28	0.30	0.35	0.13	0.08	0.03	15.27	43.04		1.2

K	source	>20	>10	>1	>0.1	>0.01	<0.01

Naming convention: U – upstream, D – downstream, S – canyon side, C – canyon centre, L – lower room, M – middle room, T – top room.

Table 5
Normalised pollutant concentrations (K) in case 2.

Source / Target		Upstream						Downstream						ACH_{PFR} (h⁻¹)
		USL	USM	UST	UCL	UCM	UCT	DSL	DSM	DST	DCL	DCM	DCT	
Upstream	USL		0.02	0.00	0.00	0.00	0.00	0.00	0.00	0.00	0.00	0.00	0.00	2.6
	USM	0.01		0.04	0.00	0.00	0.00	0.00	0.00	0.00	0.00	0.00	0.00	3.6
	UST	0.00	0.38		0.00	0.00	0.00	0.00	0.00	0.00	0.00	0.00	0.00	4.8
	UCL	0.00	0.00	0.00		0.10	0.00	0.00	0.00	0.00	0.00	0.00	0.00	7.0
	UCM	0.00	0.00	0.00	2.65		0.06	0.00	0.00	0.00	0.00	0.00	0.00	2.4
	UCT	0.00	0.00	0.00	0.92	7.80		0.00	0.00	0.00	0.00	0.00	0.00	3.3
Downstream	DSL	0.16	0.23	0.22	0.00	0.00	0.00		0.29	0.34	0.01	0.01	0.01	9.8
	DSM	0.15	0.21	0.21	0.00	0.00	0.00	4.15		0.46	0.01	0.01	0.01	13.3
	DST	0.07	0.15	0.62	0.00	0.00	0.00	4.99	0.35		0.00	0.00	0.00	8.2
	DCL	0.01	0.01	0.01	0.01	0.03	0.05	2.07	0.05	0.02		0.13	0.13	55.6
	DCM	0.01	0.02	0.02	0.03	0.09	0.15	1.21	0.08	0.05	0.19		0.26	42.5
	DCT	0.01	0.02	0.02	0.04	0.11	0.19	1.21	0.07	0.04	0.25	0.33		41.1

K | source | >20 | >10 | >1 | >0.1 | >0.01 | <0.01

Naming convention: U – upstream, D – downstream, S – canyon side, C – canyon centre, L – lower room, M – middle room, T – top room.

3.2. Ventilation case 2

In the 2nd ventilation case, the upstream building has openings on the windward side and the downstream building is cross ventilated. Table 5 summarises the inter-unit transmission of pollutants observed between each pair of rooms in this case. While this ventilation mode improves the airflow in the downstream rooms, it slightly deteriorates the air quality in the upstream building as compared to the previous configuration. Vertical transmission of pollutants is observed on the upstream building wherein the pollutants are transported from lower to upper rooms, particularly in the central rooms. Pollutants from UCL are accumulated in UCM and UCT. Similarly, pollutants from UCM are transported upwards into UCT. Interestingly, the transmission and accumulation of upstream pollutants into downstream rooms is somewhat reduced, especially near the centre of the canyon. Additionally, the airflow through the upstream rooms is significantly reduced, with an average ACH_{PFR} of 4 h⁻¹, a reduction of nearly 90% from the previous case.

On the other hand, pollutant concentration is reduced in the downstream rooms, more significantly in the central rooms (DCL, DCM and DCU). In these rooms, ventilation efficiency is simultaneously increased, with an ACH_{PFR} in the range of 10–40 h⁻¹. The greatest change is observed in the centrally located rooms (DCL, DCM and DCT), where the average ACH_{PFR} increases from 1.1 h⁻¹ (in case 1) to 46.4 h⁻¹. It is interesting to observe that the emission from DSL represents a major fraction of pollutant concentration in other downstream rooms, suggesting the influence of airflow around the canyon edges. It is possible that the superposition of the edge vortex and the canyon vortex, which results in a canyon-inward directed helical flow, transfers pollutants from DSL towards the central region. The same vortex also assists in the transportation of small amounts of pollutants from the upstream side rooms into the downstream side rooms.

Table 6
Normalised pollutant concentrations (K) in case 3.

Source / Target		Upstream						Downstream						ACH_{PFR} (h⁻¹)
		USL	USM	UST	UCL	UCM	UCT	DSL	DSM	DST	DCL	DCM	DCT	
Upstream	USL		0.04	0.00	0.00	0.00	0.00	0.00	0.00	0.00	0.00	0.00	0.00	1.0
	USM	0.02		0.06	0.00	0.00	0.00	0.00	0.00	0.00	0.00	0.00	0.00	3.0
	UST	0.00	0.77		0.00	0.00	0.00	0.00	0.00	0.00	0.00	0.00	0.00	4.3
	UCL	0.00	0.00	0.00		2.03	0.01	0.00	0.00	0.00	0.00	0.00	0.00	1.1
	UCM	0.00	0.00	0.00	19.76		0.09	0.00	0.00	0.00	0.00	0.00	0.00	1.9
	UCT	0.00	0.00	0.00	7.00	19.55		0.00	0.00	0.00	0.00	0.00	0.00	3.2
Downstream	DSL	0.37	0.41	0.33	0.01	0.01	0.01		2.99	0.33	0.03	0.02	0.02	0.6
	DSM	0.33	0.36	0.30	0.01	0.01	0.01	11.40		0.43	0.03	0.03	0.02	0.8
	DST	0.28	0.31	0.27	0.01	0.01	0.01	4.65	8.03		0.04	0.03	0.02	0.9
	DCL	0.03	0.03	0.03	0.18	0.18	0.18	0.13	0.09	0.03		1.02	0.56	0.8
	DCM	0.03	0.03	0.03	0.19	0.20	0.20	0.13	0.09	0.03	66.50		1.13	1.4
	DCT	0.02	0.03	0.03	0.22	0.24	0.25	0.12	0.08	0.03	19.11	51.03		1.1

K | source | >20 | >10 | >1 | >0.1 | >0.01 | <0.01

Naming convention: U – upstream, D – downstream, S – canyon side, C – canyon centre, L – lower room, M – middle room, T – top room.

3.3. Ventilation case 3

The 3rd case represents single-sided ventilation on both buildings, in which all rooms are open to air exchange from the face opposite to the street canyon. The ventilation mode on the upstream building is the same as in case 2 while the downstream building follows case 1. Corollary, the major routes of inter-unit pollutant transmission are expected to be the same as those observed in previous instances. Pollutants from downstream rooms are primarily transported upwards into the upper rooms (see Table 6), such as from DCL to DCM and DCT. A small quantity of pollutants is transmitted and accumulated horizontally along-the-street into other downstream rooms ($K < 0.1$). As expected, there is no transmission of pollutants from downstream to upstream rooms (across-the-street) since the windows on the downstream building face the downwind direction. The transmission pattern from upstream rooms generally stays the same as it did in case 2, albeit with slightly higher concentrations. In terms of ventilation efficiency, all rooms exhibit poor airflow with an ACH_{PFR} in the range of 0.6–4.3 h^{-1}; although the upstream rooms show a slightly higher air change rate.

3.4. Ventilation case 4

This case represents single-sided ventilation, from the street side, for both buildings. It represents a scenario with low ACH_{PFR} and high transmission, as shown in Table 7. Primarily, vertical transmission is observed for both sets of rooms, with an upward transmission in the upstream building and a downward transmission in the downstream building. For instance, the room UCT is heavily contaminated with pollutants from UCM ($K = 101.9$), and UCM is majorly contaminated with pollutants from UCL ($K = 75.25$). In contrast, pollutants from the room DCT are transported into DCM ($K = 69.34$), and pollutants from DCM are transported into DCL ($K = 69.76$).

Secondly, a strong horizontal transmission and accumulation of pollutants is observed. Pollutants from the side rooms are transported to central rooms in both buildings. Similarly, pollutants from downstream central rooms (DCL, DCM and DCT) are transported to upstream central rooms (UCL, UCM and UCT). It is worth noting, that the only routes along which little to no transmission occurs is from centre to side rooms (along-the-street). As can be seen by the four light-coloured blocks in Table 7.

In terms of ventilation efficiency, the ACH_{PFR} is quite low for all rooms with an average value of less than 2 h^{-1}. In fact, the downstream building exhibits slightly better ventilation as compared to the upstream building. The average ACH_{PFR} on the downstream building is 1.6 h^{-1}, while the upstream building has an average ACH_{PFR} of 1.1 h^{-1}. This also relates to higher pollutant cross-transmission into upstream rooms as against downstream rooms.

Table 7
Normalised pollutant concentrations (K) in case 4.

Source / Target		USL	USM	UST	UCL	UCM	UCT	DSL	DSM	DST	DCL	DCM	DCT	ACH_{PFR}
		Upstream						Downstream						
Upstream	USL		1.91	1.33	0.00	0.00	0.00	0.28	0.26	0.51	0.00	0.00	0.00	1.7
	USM	51.42		1.78	0.00	0.00	0.00	0.35	0.38	0.83	0.00	0.00	0.00	1.9
	UST	23.42	69.10		0.00	0.00	0.00	0.43	0.52	1.27	0.00	0.00	0.00	1.4
	UCL	0.70	0.80	0.80		1.36	1.04	2.79	2.67	2.10	12.25	10.44	7.16	0.5
	UCM	0.34	0.39	0.39	75.25		1.78	1.35	1.30	1.02	20.62	17.85	12.50	0.5
	UCT	0.23	0.26	0.26	28.99	101.90		0.92	0.88	0.70	16.63	15.54	12.42	0.7
Downstream	DSL	1.88	2.15	1.73	0.00	0.00	0.00		0.23	0.36	0.00	0.00	0.00	1.8
	DSM	2.25	3.22	3.65	0.00	0.00	0.00	0.11		3.53	0.00	0.00	0.00	2.0
	DST	2.10	2.92	3.69	0.00	0.00	0.00	0.13	0.16		0.00	0.00	0.00	3.1
	DCL	0.12	0.13	0.13	2.64	2.73	2.28	0.45	0.43	0.34		69.76	25.98	0.4
	DCM	0.09	0.10	0.10	2.98	3.12	2.70	0.34	0.32	0.26	4.61		69.34	0.9
	DCT	0.07	0.08	0.08	2.69	2.95	2.76	0.28	0.27	0.21	2.77	3.15		1.5

K	source	>20	>10	>1	>0.1	>0.01	<0.01

Naming convention: U – upstream, D – downstream, S – canyon side, C – canyon centre, L – lower room, M – middle room, T – top room.

Table 8
Normalised pollutant concentrations (K) in case 5.

Source Target		Upstream						Downstream						ACH_{PFR}
		USL	USM	UST	UCL	UCM	UCT	DSL	DSM	DST	DCL	DCM	DCT	
Upstream	USL		0.00	0.00	0.00	0.00	0.00	0.00	0.00	0.00	0.00	0.00	0.00	38.0
	USM	0.00		0.00	0.00	0.00	0.00	0.00	0.00	0.00	0.00	0.00	0.00	46.3
	UST	0.00	0.00		0.00	0.00	0.00	0.00	0.00	0.00	0.00	0.00	0.00	49.5
	UCL	0.00	0.00	0.00		0.00	0.00	0.00	0.00	0.00	0.00	0.00	0.00	76.4
	UCM	0.00	0.00	0.00	0.00		0.00	0.00	0.00	0.00	0.00	0.00	0.00	74.9
	UCT	0.00	0.00	0.00	0.00	0.00		0.00	0.00	0.00	0.00	0.00	0.00	68.0
Downstream	DSL	0.46	0.49	0.47	0.04	0.03	0.02		0.32	0.40	0.04	0.03	0.03	9.0
	DSM	0.46	0.48	0.47	0.05	0.03	0.02	0.32		0.56	0.04	0.03	0.03	12.5
	DST	2.20	2.92	3.98	0.00	0.00	0.00	0.26	0.33		0.00	0.00	0.00	9.3
	DCL	0.05	0.06	0.06	0.20	0.22	0.24	0.08	0.08	0.05		0.21	0.22	42.0
	DCM	0.05	0.05	0.06	0.23	0.25	0.27	0.08	0.08	0.05	0.22		0.25	41.4
	DCT	0.05	0.05	0.05	0.28	0.32	0.37	0.08	0.07	0.04	0.27	0.30		40.0

K | source | >20 | >10 | >1 | >0.1 | >0.01 | <0.01

Naming convention: U – upstream, D – downstream, S – canyon side, C – canyon centre, L – lower room, M – middle room, T – top room.

3.5. Ventilation case 5

Case 5, representing cross-ventilation on both buildings, shows high ACH_{PFR} and low transmission of pollutants (see Table 8). Opening windows on both sides of the building ensures good airflow through the rooms, with an average ACH_{PFR} of 25 h^{-1} and 59 h^{-1} in the downstream and upstream rooms, respectively. While there is negligible transmission of pollutants in the upstream rooms, there is still some degree of cross-transmission of pollutants present in the downstream rooms. In contrast to the previous ventilation cases, no significant vertical transmission is observed in this case. Rather, pollutants are transported horizontally in the streamwise direction (across-the-street) and in the spanwise direction (along-the-street). Pollutants from the upstream side rooms (USL, USM and UST) are transmitted into downstream rooms across the street (DSL, DSM and DST) and also along the canyon into the centre (DCL, DCM and DCT), albeit in smaller measure. Similarly, the upstream central rooms also contribute to the pollution in rooms across the street (DCL, DCM and DCT) as well as along the street (DSL, DSM and DST). Vertical inter-unit transmission occurs only slightly ($K = 0.2 \sim 0.5$) between the downstream rooms. For instance, pollutants from DSM are transported into both the lower and upper rooms, DSL and DST respectively.

3.6. Ventilation case 6

Case 6 represents a scenario when the upstream building is ventilated from the street side and the downstream building is cross ventilated. Primarily, inter-unit pollutant transmission occurs in the vertical direction near the upstream building (see Table 9). Pollutants released from the lower rooms are transported upwards, contaminating the rooms above. For instance, pollutants from the

Table 9
Normalised pollutant concentrations (K) in case 6.

Source Target		Upstream						Downstream						ACH_{PFR}
		USL	USM	UST	UCL	UCM	UCT	DSL	DSM	DST	DCL	DCM	DCT	
Upstream	USL		1.15	0.71	0.00	0.00	0.00	0.22	0.22	0.07	0.00	0.00	0.00	1.7
	USM	36.08		0.90	0.00	0.00	0.00	0.26	0.30	0.10	0.00	0.00	0.00	2.0
	UST	14.71	48.42		0.00	0.00	0.00	0.31	0.40	0.15	0.00	0.00	0.00	1.6
	UCL	0.27	0.32	0.29		0.38	0.25	1.63	1.48	0.17	28.25	8.58	5.33	0.7
	UCM	0.09	0.11	0.10	70.11		0.36	0.57	0.52	0.06	20.93	12.19	7.72	0.9
	UCT	0.04	0.05	0.05	10.77	26.49		0.28	0.26	0.03	8.56	7.62	5.73	1.5
Downstream	DSL	0.36	0.38	0.32	0.00	0.00	0.00		0.20	0.47	0.00	0.01	0.01	7.4
	DSM	0.34	0.36	0.31	0.00	0.00	0.00	0.23		0.53	0.01	0.01	0.01	10.1
	DST	1.42	2.11	2.42	0.00	0.00	0.00	0.11	0.15		0.00	0.00	0.00	10.3
	DCL	0.02	0.02	0.02	0.10	0.09	0.07	0.05	0.05	0.02		0.21	0.22	34.2
	DCM	0.03	0.03	0.02	0.11	0.10	0.08	0.07	0.06	0.03	0.22		0.23	38.1
	DCT	0.03	0.03	0.03	0.13	0.12	0.10	0.08	0.08	0.03	0.26	0.26		39.6

K | source | >20 | >10 | >1 | >0.1 | >0.01 | <0.01

Naming convention: U – upstream, D – downstream, S – canyon side, C – canyon centre, L – lower room, M – middle room, T – top room.

room USL are transmitted into USM ($K = 36.08$) and UST ($K = 14.71$), while pollutants from UCL are mainly transmitted and accumulated in UCM (K =$K = 70.11$) and UCT ($K = 10.77$). The other transmission route of concern is the streamwise (across-the-street) flow of pollutants near the centre of the canyon. Assisted by the recirculating vortex, pollutants released from downstream central rooms (DCL, DCM and DCT) are transported into upstream central rooms (UCL, UCM and UCT) in the range $K = [5, 30]$. The upstream rooms also demonstrate low levels of ACH_{PFR} (<2 h^{-1}), being ventilated from the leeward side. In fact, central upstream rooms have even lower ACH_{PFR} (<1.5 h^{-1}), leading to higher transmission and accumulation of adventitious pollutants in them.

Additionally, pollutants from upstream side rooms are transported across-the-street into downstream rooms in lower concentrations ($K < 1$), however, accumulation of pollutants on the top floor can exceed K = 2. In the case of downstream building, vertical transmission of pollutants is not very prominent, and transmission occurs generally in all directions at a reduced concentration ($K < 1$), apart from the critical scenario near the centre of the canyon ($K > 20$). Finally, negligible transmission occurs from central to side rooms for both the upstream and downstream building. In terms of ventilation efficiency, the downstream rooms have $ACH_{PFR} \approx 10$ h^{-1}, and >30 h^{-1} for the side and central rooms, respectively. The higher air changes at the centre of the canyon also explain why the rooms, in that location, have lower concentrations of transmitted pollutants when compared to the side rooms.

3.7. Ventilation case 7

Ventilation case 7 represents a scenario where the upstream rooms are cross-ventilated and downstream rooms are ventilated from the street facing façade. Table 10 shows the normalised concentrations of transmitted pollutants. As is expected, transmission of pollutants into upstream rooms is negligible, due to the high ventilation rate through the rooms ($ACH_{PFR} > 38$ h^{-1}). Instead, pollutants from the upstream rooms are transported into downstream rooms, primarily across the street. For instance, pollutants from UCL are transported across the street into DCL ($K = 46.71$), DCM and DCT ($K < 10$). Simultaneously, small concentration of pollutants from upstream side rooms is transmitted and accumulated in downstream central rooms ($K < 0.1$).

Table 10
Normalised pollutant concentrations (K) in case 7.

Source Target		USL	USM	UST	UCL	UCM	UCT	DSL	DSM	DST	DCL	DCM	DCT	ACH_{PFR}
Upstream	USL		0.00	0.00	0.00	0.00	0.00	0.00	0.00	0.00	0.00	0.00	0.00	38.4
	USM	0.00		0.00	0.00	0.00	0.00	0.00	0.00	0.00	0.00	0.00	0.00	46.0
	UST	0.00	0.00		0.00	0.00	0.00	0.00	0.00	0.00	0.00	0.00	0.00	48.2
	UCL	0.00	0.00	0.00		0.00	0.00	0.00	0.00	0.00	0.00	0.00	0.00	74.6
	UCM	0.00	0.00	0.00	0.00		0.00	0.00	0.00	0.00	0.00	0.00	0.00	74.6
	UCT	0.00	0.00	0.00	0.00	0.00		0.00	0.00	0.00	0.00	0.00	0.00	68.7
Downstream	DSL	1.65	2.31	2.49	0.00	0.00	0.00		0.57	0.55	0.00	0.00	0.00	1.9
	DSM	2.17	3.04	4.10	0.00	0.00	0.00	0.12		5.87	0.00	0.00	0.00	2.3
	DST	2.16	2.78	3.89	0.00	0.00	0.00	0.16	0.20		0.00	0.00	0.00	3.1
	DCL	0.02	0.03	0.03	46.71	11.30	2.25	0.06	0.07	0.06		6.30	7.31	0.8
	DCM	0.02	0.02	0.02	6.57	10.39	3.54	0.04	0.05	0.04	10.96		32.98	0.8
	DCT	0.01	0.02	0.02	1.95	3.39	4.18	0.03	0.04	0.04	0.98	1.40		1.3

K	source	>20	>10	>1	>0.1	>0.01	<0.01

Naming convention: U – upstream, D – downstream, S – canyon side, C – canyon centre, L – lower room, M – middle room, T – top room.
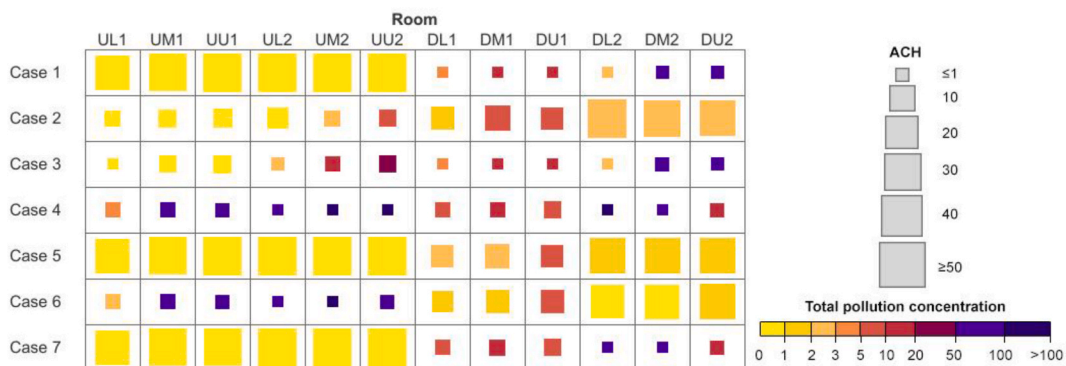
Fig. 8. Relation between ACH and total transmitted pollutants.

On the other hand, pollutants released in the downstream rooms are transmitted vertically, with higher pollutant accumulation in the central rooms. Interestingly, vertical transmission of pollutants from downstream side rooms has remained low for all ventilation scenarios described previously. The ventilation rate is also quite poor in the downstream rooms, especially in the central ones, which indicates that adventitious pollutants reside longer in them and, hence, explain the higher concentrations.

3.8. Comparison of extreme cases

Fig. 8 shows the relationship between ACH_{PFR} and total pollutant concentration in each room. The size of the square indicates the air changes in the room, while the colour indicates the sum of all adventitious pollutant concentrations in the room. Note that this is different from the pollutant concentration values presented earlier, which was the concentration of pollutants from individual rooms. A large ACH_{PFR} prevents build-up of pollutants and restricts cross-transmission and accumulation between the rooms, demonstrated by the yellow-to-orange shade of the large squares. Downstream rooms in cases 2 and 5, and upstream rooms in cases 1 and 5 record low levels of inter-unit transmission accompanied by the highest air changes. The inverse does not hold true for all cases, i.e., low air changes in a room do not necessarily lead to cross-transmission, although it is an important criterion for inter-unit transmission and accumulation of pollutants. Upstream rooms in case 4 demonstrate low ACH_{PFR} and high transmission, while upstream rooms in case 2 demonstrate low ACH_{PFR} and low pollution. In general, it can be said that apart from the source location, improving the ventilation efficiency in the indoor space can reduce the built-up of cross-transmitted pollutants, indicated by a correlation coefficient of -0.36 between the ACH_{PFR} and the total adventitious pollutant concentration. Similar findings were also reported by Wang et al. [22], who showed that increasing the ventilation rate reduced the transmission of pollutants in a single-side ventilated multistorey building. Additionally, the range of predicted ACH, [0.4 h^{-1}, 7 h^{-1}] and [9 h^{-1}, 76 h^{-1}] for single-sided and cross ventilation scenarios, respectively, fall within the range of real-world observations [93].

Cases 4 and 5 represent the extreme ventilation modes, with the room-averaged total pollutant concentration of 61.6 and 1.6, respectively. We have so far discussed the inter-unit transmission for individual ventilation cases, however, to understand the broader aspect of inter-unit transmission and the impact of these two extreme ventilation scenarios, further discussion is necessary. Table 11 shows the contours of normalised pollutant concentration through the central rooms. The colour scale has been readjusted for clarity.

From Table 11 and it can be inferred that inter-unit transmission predominantly occurs in the single-sided ventilation mode (case 4). The presence of a strong vortex in the street canyon (in case 4) causes the recirculation of pollutants and their subsequent re-entry into other rooms, which can be visualised in the velocity streamline figure. The exhausted pollutants from the upstream rooms are pushed upwards, and the pollutants from downstream rooms are pushed downwards. Vertical transmission into adjacent rooms is in the range of $K = [50 \text{ to } 100]$ and represents the main inter-unit transmission route. The skimming airflow also transports some of the pollutants into the rooms across the street. Sources of pollutants located downstream cause a moderate degree of inter-unit transmission in the upstream rooms, as seen in the results presented in Table 11 (single-sided ventilation – DCL, DCM and DCT), with normalised pollutant concentration in the range of $K = [10 \text{ to } 50)$. The height of the source room is also critical. Lower rooms on upstream building and upper rooms on the downstream building are relatively more contagious, transmitting their pollutants into more rooms. For instance, the room DCT affects the air quality of all the rooms in the neighbourhood, as compared to DCL.
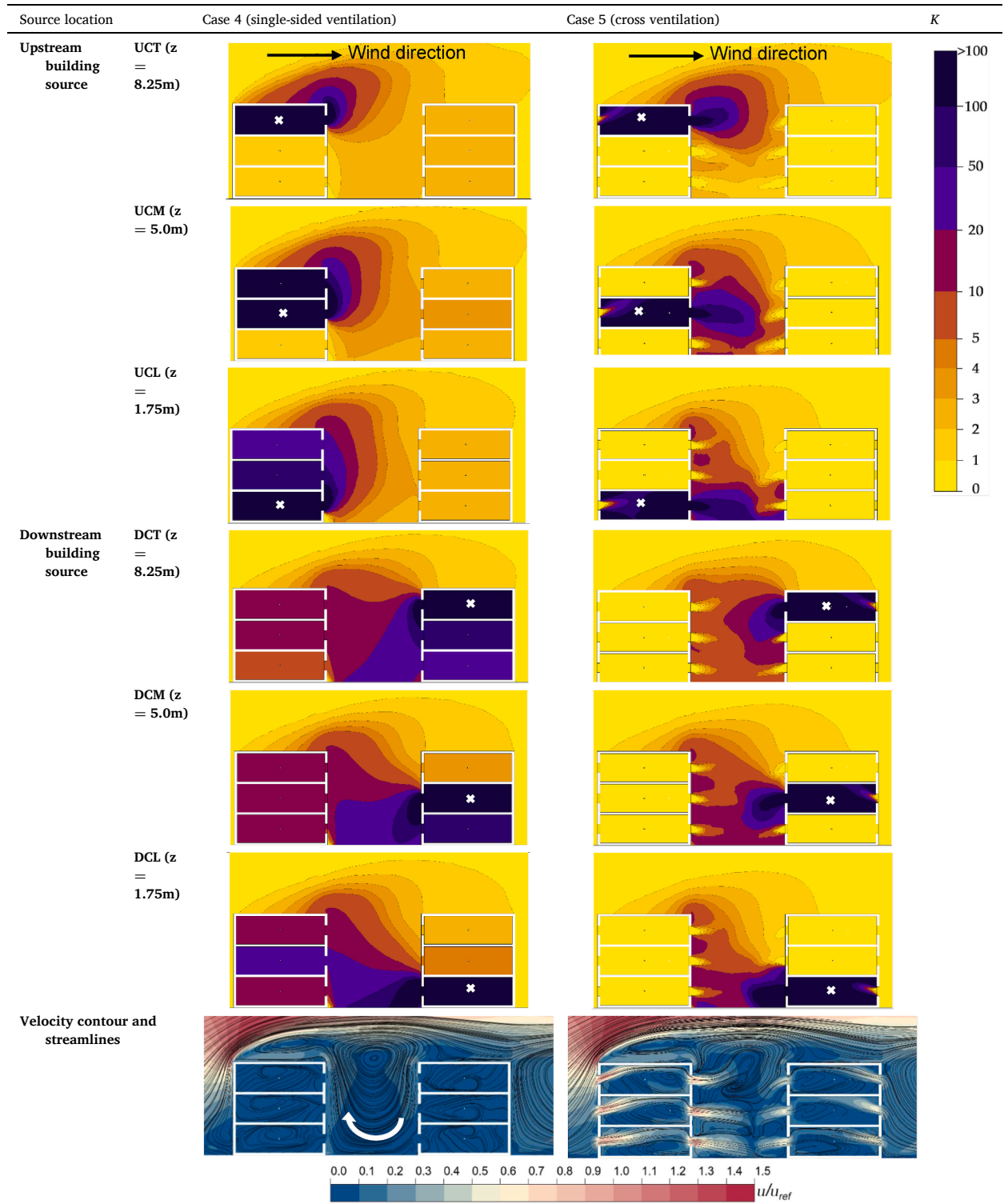
In contrast, transmission routes for upstream sources are primarily in the vertical direction, followed by low levels of transmission into rooms across the street (DCT, DCM and DCL) with $K < 5$. This can be explained by the interaction of the canyon vortex with the freestream airflow above the canyon, which dilutes the pollutant concentration.

The benefits of opening windows on opposite sides of a room are multiple, as demonstrated by the results of the cross-ventilation mode (case 5) in Table 11. This mode of ventilation enables crossflow of air across the rooms, leading to a reduction in cross-transmission and accumulation of pollutants in the neighbouring rooms as well as improved ACH_{PFR}. The velocity streamline figure indicates that the air flows towards the street canyon as it passes through the rooms, resulting in minimal accumulation of cross-transmitted pollutants. As a result, the normalised concentration of any cross-transmitted pollutant remains below one ($K < 1$). This demonstrates the effectiveness of cross-ventilation in reducing inter-unit transmission of pollutants and improving indoor air quality.

Table 12 shows the contours of normalised pollutant concentration along the side rooms, along with the velocity streamlines. Cross-transmission of pollutants is generally lower here than at the centre of the canyon. The impact of downstream pollutant sources on the upstream air quality is reduced in this zone. On the contrary, upstream pollutants are more dispersed, polluting other rooms in the process. In fact, upstream sources of pollutants impact the air quality of neighbouring rooms in both the upstream and downstream buildings, regardless of the ventilation mode.
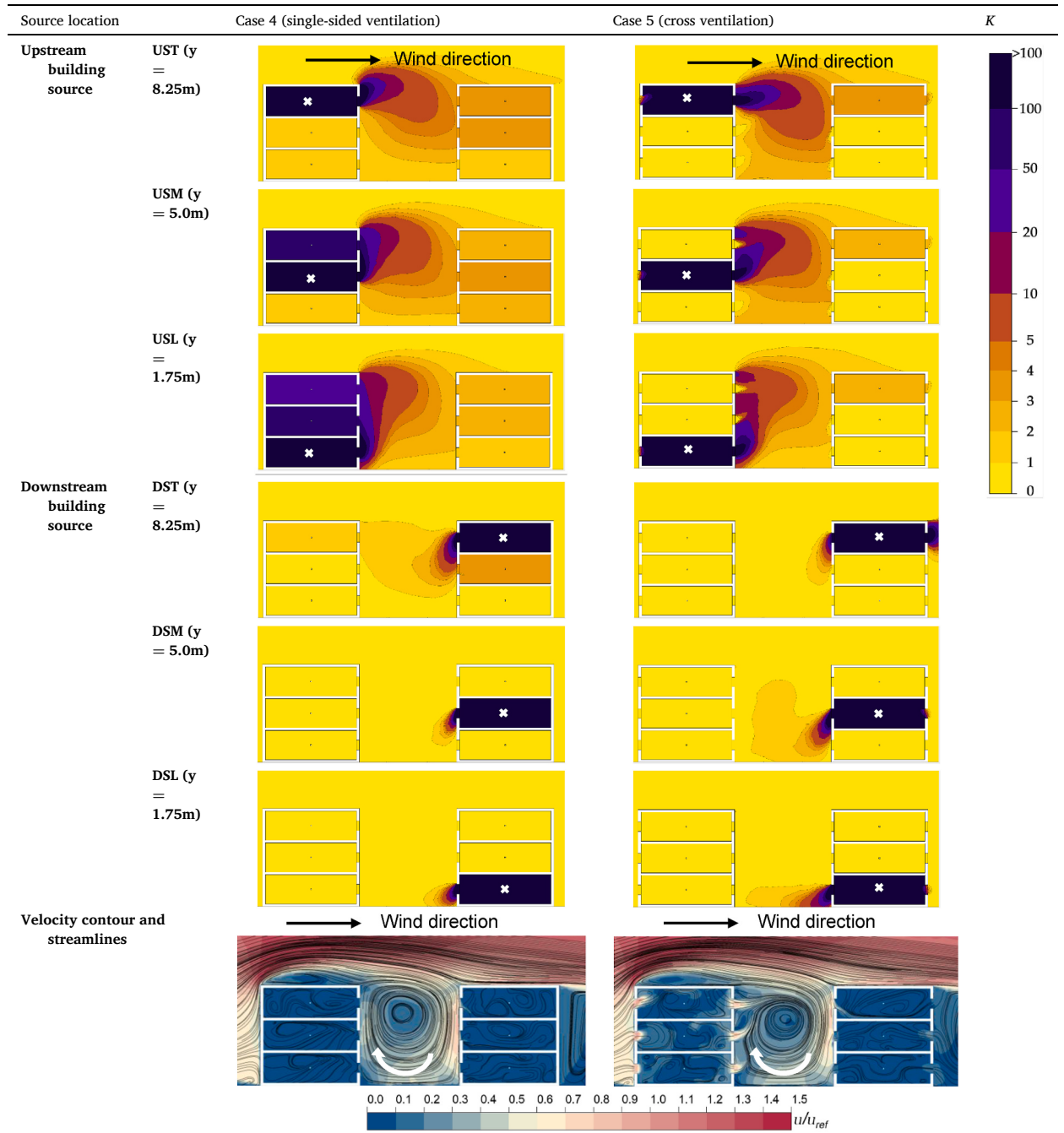
In the single-sided ventilation mode, the primary transmission route is in the vertical direction, aided by the recirculating vortex in the street. However, due to the presence of corner eddies, which aids in the dispersion of the pollutants, the inter-unit transmission in

Table 11

Contours of normalised pollutant concentration (K) and velocity streamlines through the central rooms.

Source location		Case 4 (single-sided ventilation)	Case 5 (cross ventilation)	K
Upstream building source	**UCT (z = 8.25m)**			
	UCM (z = 5.0m)			
	UCL (z = 1.75m)			
Downstream building source	**DCT (z = 8.25m)**			
	DCM (z = 5.0m)			
	DCL (z = 1.75m)			
Velocity contour and streamlines				

Table 12

Contours of normalised pollutant concentration (K) and velocity streamlines through the side rooms.

Source location		Case 4 (single-sided ventilation)	Case 5 (cross ventilation)	K
Upstream building source	**UST (y = 8.25m)**			
	USM (y = 5.0m)			
	USL (y = 1.75m)			
Downstream building source	**DST (y = 8.25m)**			
	DSM (y = 5.0m)			
	DSL (y = 1.75m)			
Velocity contour and streamlines				

the streamwise direction (across the street) is much lower compared to the central rooms. Interestingly, when the building is cross-ventilated, transmission of pollutants occurs only in the room DST regardless of the source location in the upstream building. This is because airflow in room DST is from the street side rather than the leeward face as is the case in rooms DSM and DSL. The airflow in the street picks up pollutants from the canyon and carries them into the room DST. This can be visualised by the downward flow of air near the left window in DST (see velocity streamline diagram in Table 12). In contrast to the DST, the other downstream rooms (DSM and DSL) have a lower concentration of pollutants that are transmitted and accumulated into the space from the leeward face of the building. This occurs due to the presence of an additional recirculation zone in the wake of the building.

The analysis so far has highlighted two routes of inter-unit pollutant transmission which impact indoor air quality. The first route is
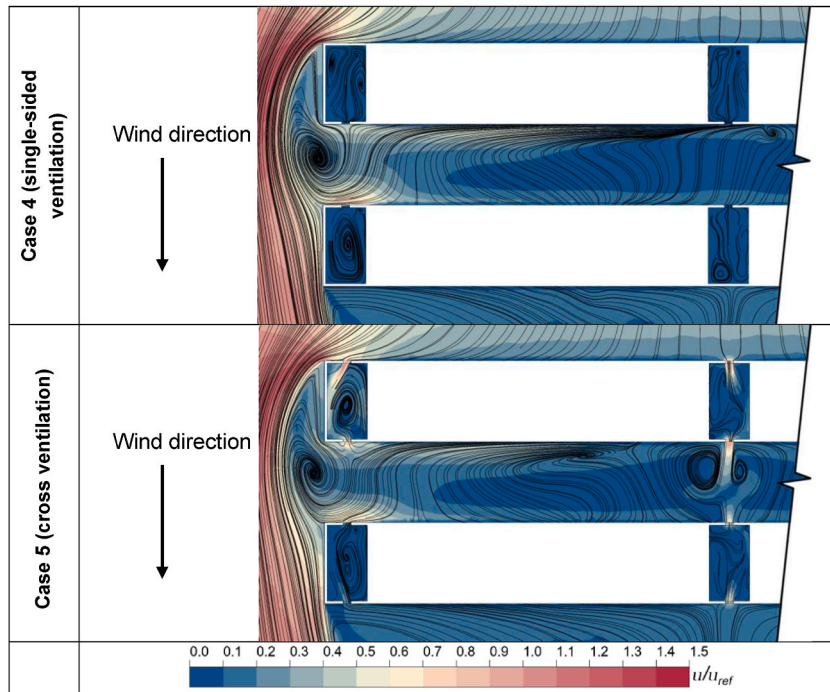
Fig. 9. Velocity contour and streamline along a horizontal plane at mid-height of the building (only half of the canyon is shown for clarity).

the vertical transmission which transports the bulk of pollutants from the source room ($K > 20$), if the room is not cross-ventilated. The second route of transmission is across-the-street (streamwise transmission), with a reduced pollutant concentration ($K = [0.2$ to $20]$). Both these routes are impacted by the recirculating vortex in the canyon. However, the presence of corner eddies, which rotate around a vertical axis, introduces a third inter-unit transmission route which is less pronounced, but nevertheless crucial for building ventilation design. This transmission occurs along-the-street (spanwise transmission) and is driven by the corner eddies identified in Fig. 9, which shows the velocity contours and streamlines at the mid-height of the building. A similar flow structure has been identified by other studies, including Gromke and Ruck [94].

The streamlines indicate that the corner vortices drive air towards the centre of the canyon along with the released pollutants. In the case of single-sided ventilation, because the ventilation occurs from the street side, some of the pollutants are transmitted into the central rooms. This route of transmission is demonstrated in Table 7 as well, where rooms USL, USM and UST transmit pollutants into rooms UCL, UCM, UCT, DCL, DCM and DCT ($K = [0.08$ to $0.8]$). Similarly, transmission from the rooms DSL, DSM and DST into central rooms is also observed. On the other hand, the risk of inter-unit transmission from the side to central rooms is much lower in the case of cross-ventilation as the flow field is highly 3-dimensional near the centre of the canyon (with $K \approx 0.03$). Additionally, the airflow through the central rooms is primarily from the face opposite the canyon.

There are several implications to the observed transmission routes. Namely, the central rooms are more susceptible to contamination by adventitious pollutants, especially when ventilated from a single side. As expected, the recirculating vortices inside the canyon and at the edges accumulate pollutants near the centre of the canyon, increasing the risk of transmission into the rooms there. Fig. 10(a) explains this with the example of room DCT as a source, under the specific scenario of single-sided ventilation from street canyon. The released pollutants are largely transported to central rooms, below and across the street. On the contrary, the side rooms are more contagious than central room, in the sense that pollutants released from the side rooms are transported along the length of the canyon increasing the risk of inter-unit transmission in all rooms. While the actual pollutant concentration is low, it is nevertheless higher than the transmission from central to side rooms. Fig. 10(b) demonstrates the transmission routes from the room UST, under the influence of cross-ventilation. The choice of ventilation case 5 highlights that even with an improved air flow through the rooms, there is still some transmission and accumulation of pollutants from the side rooms into the central rooms. In fact, other ventilation cases show higher transmission along this route.
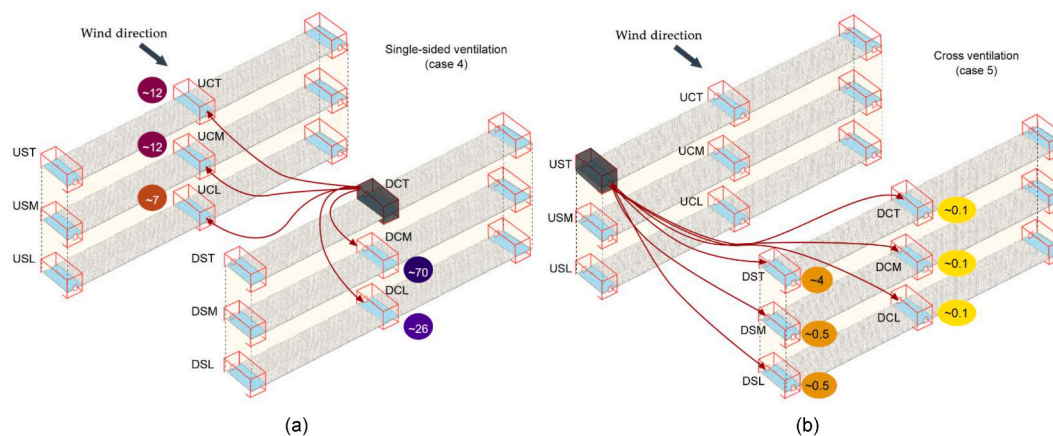
Fig. 10. Inter-unit transmission routes, (a) Ventilation case 4 with DCT as source room, (b) Ventilation case 5 with UST as source room.

4. Conclusions and recommendations for future research

Pollutants originating from an indoor room can have a significant impact on the wellbeing of residents in neighbouring rooms/ apartments along the street. This study aimed to understand the inter-unit transmission of pollutants in an isolated street canyon under a perpendicular wind flow. A CFD model was created to simulate air flow and pollution dispersion from the internal rooms, which was validated against two experimental results. The study considered seven ventilation strategies, each representing a different window opening combination on the two buildings. Normalised pollutant concentrations inside the rooms and outdoor air flow were analysed. The main insights drawn from the results are discussed below.

- The window opening strategy was found to be instrumental in influencing the pattern of air change rates. Cross ventilation amplified the ACH_{PFR} within the central rooms, whereas single-sided ventilation favoured those located at the street corners. Furthermore, the accumulation of transmitted pollutants was significantly affected by a room's location and air exchange rate, resulting in higher accumulation in the central rooms and those with low ACH_{PFR}. Notably, a negative correlation coefficient (-0.3) exists between pollutant concentration and ACH_{PFR}.
- The downstream rooms were typically more susceptible to pollutant accumulation and inter-unit transmission, except for cases 4 and 6, where upstream rooms saw a greater accumulation due to the presence of an undisturbed vortex near the centre of the canyon. Pollutants from central rooms tend to accumulate within the central rooms, while those from side rooms spread along the length of the street, leading to inter-unit transmission in both central and side rooms, albeit at low concentrations.
- Three routes of inter-unit pollutant transmission in street canyons were identified: vertical transmission, streamwise transmission (across the street) and spanwise transmission (along the street), listed in decreasing order of relevance.

Our findings present new insights within the domain of indoor-outdoor air interaction, shedding light on the interplay between room location and potential inter-unit pollutant transmission. In addition, the pressure measurement results from the wind tunnel experiment provide a valuable resource for other researchers aiming to validate numerical simulations for building engineering applications. The study was limited to the exploration of wind-driven transmission characteristics. Future investigations should consider a range of environmental and urban variables, such as building configurations and urban elements, including vegetation and vehicles. Follow-up investigations, utilising methods such as tracer gas analysis and transient simulations, promise to provide enhanced insights that can guide urban planners in devising targeted intervention strategies for ensuring healthier indoor environments.

Author statement

Murtaza Mohammadi: Conceptualization, Methodology, Software, Validation, Data curation, Formal analysis, Investigation, Visualization, Writing- Original draft preparation. John Kaiser Calautit: Conceptualization, Formal analysis, Investigation, Writing- Reviewing and Editing, Funding acquisition, Supervision. John S. Owen: Writing- Reviewing and Editing, Resources, Supervision. Christof Gromke: Writing- Reviewing and Editing, Methodology, Investigation, Formal analysis, Supervision. Yupeng Wu: Writing- Reviewing and Editing, Supervision. Hao Liu: Writing- Reviewing and Editing, Supervision, Funding acquisition, Project administration, Resources.

Declaration of competing interest

The authors declare that they have no known competing financial interests or personal relationships that could have appeared to influence the work reported in this paper.

Data availability

Data will be made available on request.

Acknowledgement

Appendix A

A grid verification study was conducted for the idealised street canyon model, without the internal rooms. For this purpose, three grids of increasing fineness were created. The coarse mesh had 0.95 million cells, the medium mesh had 1.8 million cells and the fine mesh had 9.5 million cells. Normalised velocity at different heights at the centre of the canyon was selected as the variable for comparison (Fig. A1). The Grid Convergence Index (GCI) was calculated as outlined by Celik et al. [97] with a factor of safety equal to 1.25.
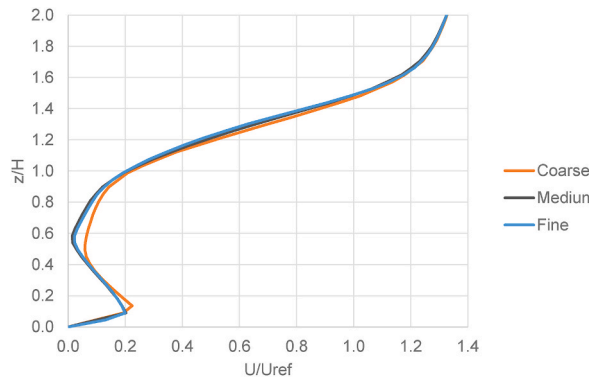
Fig. A1. Grid verification

Table A1 shows the sample GCI calculation for the mean velocity and the velocity at the point of maximum discretisation error. The φ is the numeric value of the parameter under study, ε is the difference in the numeric value between the grids, p is the apparent order, r is the refinement factor and φ_{ext} is the extrapolated relative error. The numbers 1, 2 and 3 correspond to fine, medium and coarse grids. The reader is referred to the work by Celik et al. [95] for relevant formulations. According to Table A1 the GCI for the line-averaged U/U_{ref} was equal to 0.2%. The maximum discretisation error of 0.7% occurred at z/H = 0.6, however the global GCI calculated over z/H = 0.2, 0.4, 0.6, 0.8, 1, 1.2, 1.4, 1.6, 1.8 and 2 was equal to 0.16%. It can be inferred that the medium quality mesh can generate results at a sufficient accuracy within an acceptable error range. Besides, the required computational demand was also lower. Consequently, it was preferred for the remainder of the study. The final building model, integrated with indoor rooms, consisted of approximately 6.4 million cells.

Table A1
Sample discretisation error calculation using GCI method

Variable	φ_3 (coarse)	φ_2 (medium)	φ_1 (fine)	$\varepsilon_{21}/\varepsilon_{32}$	$\varepsilon_{32}/\varepsilon_{21}$	p	r_{12}	r_{23}	φ_{ext}^{21}	GCI_{fine}^{21}
$\overline{U}/U_{ref}$	0.012	0.032	0.034	0.090	11.048	6.522	1.72	1.25	0.013	0.2%
$U_{z/h=0.6}/U_{ref}$	0.078	0.034	0.043	0.185	5.393	6.489	1.72	1.25	0.017	0.7%

Appendix B

Fig. B1 shows the contours of pressure coefficient along the inside surface of the rooms. The internal C_p predictions by the RSM simulation closely follow the wind tunnel experiment for the downstream rooms. On the upstream room, however, the RSM turbulence model can reproduce only the top room accurately. There is some deviation for the middle and lower rooms. The flow near the upstream building is characterised by impinging, separation, vortex shedding and highly 3-dimensional in nature making it difficult to predict the flow field accurately. In fact, all four RANS models predict higher C_p on the top floor as compared to the lower floors in the upstream building.
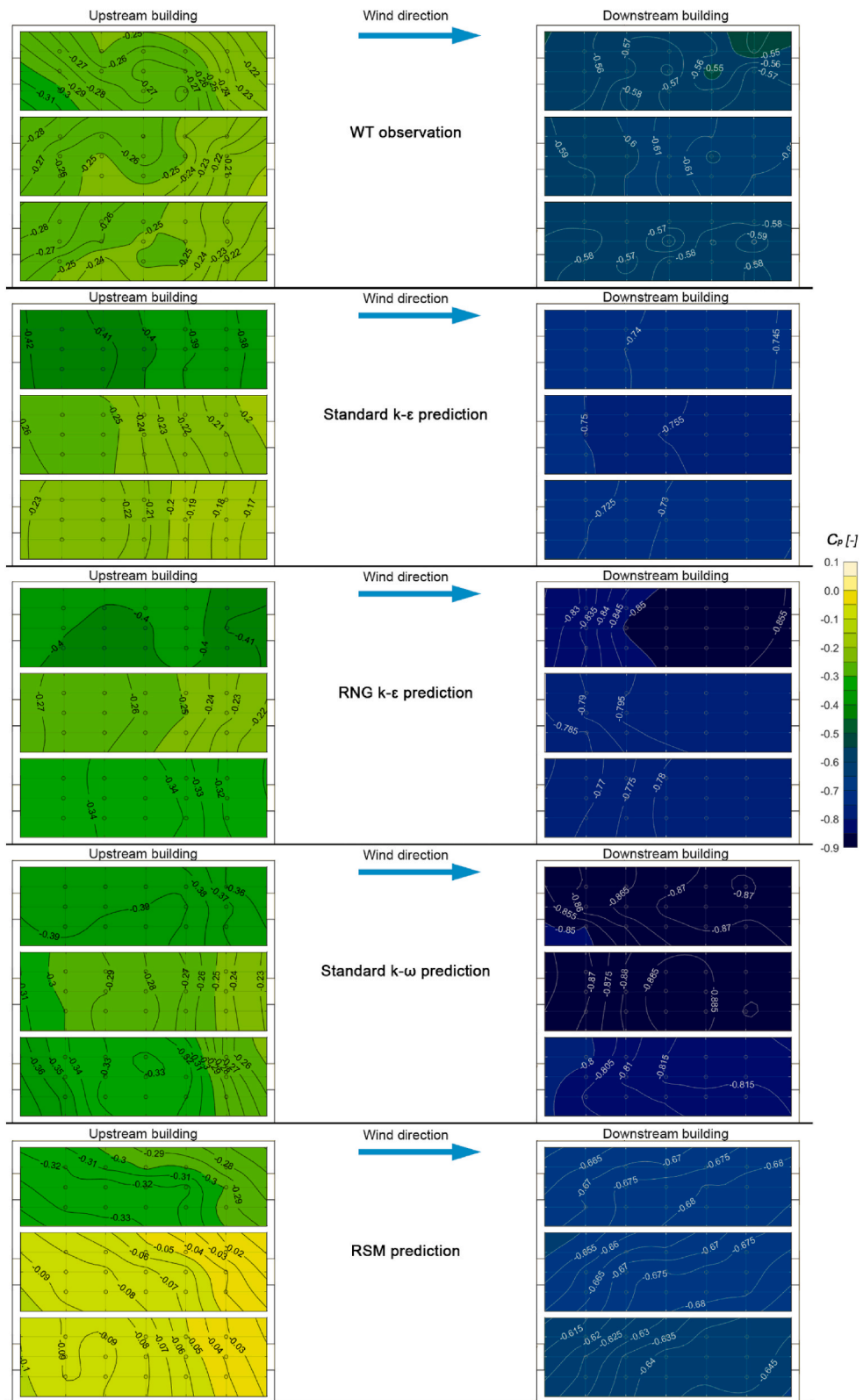
Fig. B1. A comparison of contour plots of C_p along the internal wall of the room

Fig. B2 compares the normalised vertical component of velocity ($u_z^+ = u_z/u_{ref}$), at the centre of the street canyon, between the different turbulent models. The CFD contour plots reveal qualitatively similar flow fields, despite the higher prediction of u_z^+ above the

canyon when compared to the WT. The standard k-ε closure model underestimates u_z^+ along the upstream building accompanied by overestimation on the downstream building. On the other hand, the RNG k-ε and standard k-ω demonstrate marginal improvements in capturing u_z^+ along the upstream building. In contrast, the RSM model performs significantly better in predicting the u_z^+ along both building surfaces. The deviation in the RSM u_z^+ values indicate a stronger vortex inside the canyon and consequently, higher pollutant concentration. While acknowledging that this may not precisely emulate real-world conditions, the heightened predictive capabilities of the model can be leveraged to introduce an enhanced factor of safety.
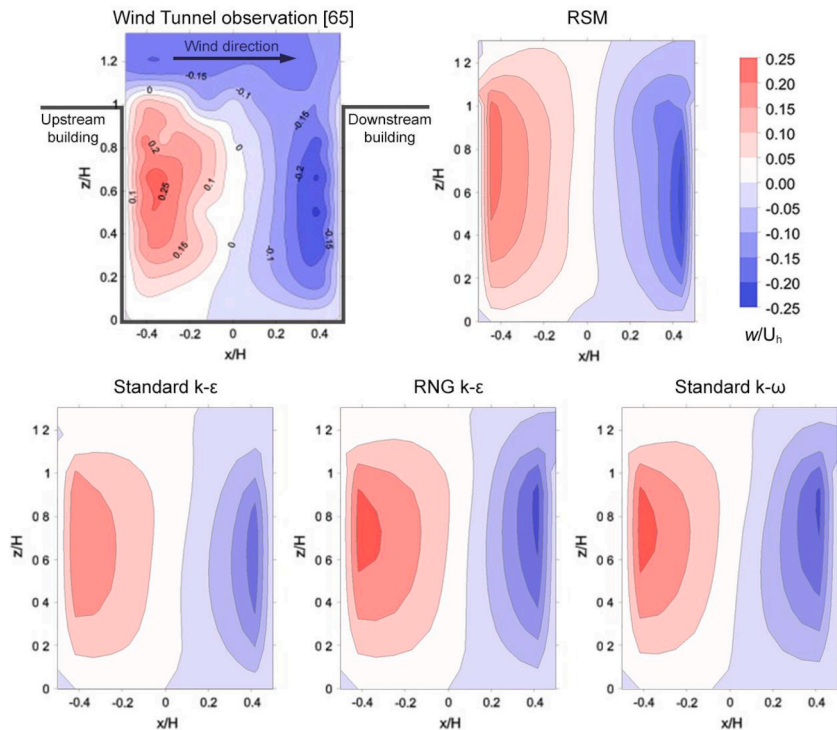
Fig. B2. A comparison of vertical velocity at the centre of the canyon for the street canyon without internal rooms

References

[1] C.J.L. Murray, et al., Global burden of 87 risk factors in 204 countries and territories, 1990-2019: a systematic analysis for the Global Burden of Disease Study 2019, Lancet (2020), https://doi.org/10.1016/S0140-6736(2030752-2).

[2] World Health Organization, World Health Statistics 2020: Monitoring Health for the SDGs, sustainable development goals., Geneva, 2020. Sep. 29, 2020, https://apps.who.int/iris/bitstream/handle/10665/332070/9789240005105-eng.pdf.

[3] Dr D.R. Boyd, The human right to breathe clean air, Ann Glob Health 85 (1) (2019), https://doi.org/10.5334/AOGH.2646.

[4] C.A. Pope, M. Ezzati, D.W. Dockery, "Tradeoffs between income, air pollution and life expectancy: brief report on the US experience, Environ. Res. 142 (Oct. 2015) 591–593, https://doi.org/10.1016/j.envres.2015.08.014, 1980-2000.

[5] J. Lelieveld, A. Pozzer, U. Pöschl, M. Fnais, A. Haines, T. Münzel, Loss of life expectancy from air pollution compared to other risk factors: a worldwide perspective, Cardiovasc. Res. 116 (11) (Sep. 2020) 1910–1917, https://doi.org/10.1093/CVR/CVAA025.

[6] N.R. Martins, G. Carrilho da Graça, A simulation study of decreased life expectancy from exposure to ambient particulate air pollution (PM2.5) in naturally ventilated workspaces, J. Build. Eng. 30 (Jul. 2020), 101268, https://doi.org/10.1016/J.JOBE.2020.101268.

[7] WHO, Review of Evidence on Health Aspects of Air Pollution – REVIHAAP Project, World Health Organization, Mar. 2013. Apr. 09, 2021, https://www.euro.who.int/en/health-topics/environment-and-health/air-quality/publications/2013/review-of-evidence-on-health-aspects-of-air-pollution-revihaap-project-final-technical-report.

[8] Department for Environment Food and Rural Affairs, The air quality strategy for england, scotland, wales and northern Ireland, Jun. 17, 2021, www.defra.gov.uk, 2007.

[9] C. Copat, et al., The role of air pollution (PM and NO2) in COVID-19 spread and lethality: a systematic review, Environ. Res. 191 (Dec. 2020), 110129, https://doi.org/10.1016/j.envres.2020.110129. Academic Press Inc.

[10] M.G. Manoj, M.K. Satheesh Kumar, K.T. Valsaraj, C. Sivan, S.K. Vijayan, Potential link between compromised air quality and transmission of the novel corona virus (SARS-CoV-2) in affected areas, Environ. Res. 190 (Nov. 2020), 110001, https://doi.org/10.1016/j.envres.2020.110001.

[11] C. Li, S. Managi, Spatial variability of the relationship between air pollution and well-being, Sustain. Cities Soc. 76 (Jan. 2022), 103447, https://doi.org/10.1016/J.SCS.2021.103447.

[12] S. Herfst, et al., Drivers of airborne human-to-human pathogen transmission, Curr Opin Virol 22 (Feb. 2017) 22–29, https://doi.org/10.1016/J.COVIRO.2016.11.006.

[13] C.C. Wang, et al., Airborne transmission of respiratory viruses, Science 373 (6558) (1979), https://doi.org/10.1126/SCIENCE.ABD9149/ASSET/9C00F9CB-FB7F-479D-BF56-5719BE0142E9/ASSETS/IMAGES/LARGE/SCIENCE.ABD9149-F5.JPG. Aug. 2021.

[14] Y. Li, S. Duan, I.T.S. Yu, T.W. Wong, Multi-zone modeling of probable SARS virus transmission by airflow between flats in Block E, Amoy Gardens, Indoor Air 15 (2) (Apr. 2005) 96–111, https://doi.org/10.1111/j.1600-0668.2004.00318.x.

[15] C. Chen, B. Zhao, C.J. Weschler, Indoor exposure to 'outdoor PM₁₀': assessing its influence on the relationship between PM₁₀ and short-term mortality in U.S. Cities on JSTOR, Epidemiology 23 (6) (2012).

[16] T.A. Kraev, G. Adamkiewicz, S.K. Hammond, J.D. Spengler, Indoor concentrations of nicotine in low-income, multi-unit housing: associations with smoking behaviours and housing characteristics, Tobac. Control 18 (6) (Dec. 2009) 438–444, https://doi.org/10.1136/TC.2009.029728.

[17] S. Xin, Q. Li, S. Liu, K. Ji, Dust dispersion patterns during building construction processes: a multi-process simulation study, J. Build. Eng. (Aug. 2023), 107478, https://doi.org/10.1016/j.JOBE.2023.107478.

[18] D. Mu, N. Gao, T. Zhu, Wind tunnel tests of inter-flat pollutant transmission characteristics in a rectangular multi-storey residential building, part A: effect of wind direction, Build. Environ. 108 (Nov. 2016) 159–170, https://doi.org/10.1016/j.buildenv.2016.08.032.

[19] D. Mu, C. Shu, N. Gao, T. Zhu, Wind tunnel tests of inter-flat pollutant transmission characteristics in a rectangular multi-storey residential building, part B: effect of source location, Build. Environ. 114 (Mar. 2017) 281–292, https://doi.org/10.1016/j.buildenv.2016.12.031.

[20] D. Mu, N. Gao, T. Zhu, CFD investigation on the effects of wind and thermal wall-flow on pollutant transmission in a high-rise building, Build. Environ. 137 (Jun. 2018) 185–197, https://doi.org/10.1016/j.buildenv.2018.03.051.

[21] X. Liu, M. Wu, Z. An, T. Chen, Study on the combined effect of wind and buoyancy on cross-unit contamination around a high-rise residential building, Sustain. Cities Soc. 82 (Jul. 2022) 103860, https://doi.org/10.1016/J.SCS.2022.103860.

[22] J. Wang, T. Zhang, S. Wang, F. Battaglia, Gaseous pollutant transmission through windows between vertical floors in a multistory building with natural ventilation, Energy Build. 153 (Oct. 2017) 325–340, https://doi.org/10.1016/j.enbuild.2017.08.025.

[23] J. Huang, P. Jones, A. Zhang, S.S. Hou, J. Hang, J.D. Spengler, Outdoor airborne transmission of coronavirus among apartments in high-density cities, Front Built Environ 0 (May 2021) 48, https://doi.org/10.3389/FBUIL.2021.666923.

[24] D. Cui, Z. Ai, C.-M. Mak, K. Kwok, P. Xue, The influence of envelope features on interunit dispersion around a naturally ventilated multi-story building Article History, Build. Simulat. 11 (16) (2018), https://doi.org/10.1007/s12273-018-0460-x.

[25] D.J. Cui, C.M. Mak, K.C.S. Kwok, Z.T. Ai, CFD simulation of the effect of an upstream building on the inter-unit dispersion in a multi-story building in two wind directions, J. Wind Eng. Ind. Aerod. 150 (Mar. 2016) 31–41, https://doi.org/10.1016/j.jweia.2016.01.007.

[26] P.Y. Cui, Y. Zhang, W.Q. Chen, J.H. Zhang, Y. Luo, Y.D. Huang, Wind-tunnel studies on the characteristics of indoor/outdoor airflow and pollutant exchange in a building cluster, J. Wind Eng. Ind. Aerod. 214 (Jul. 2021), 104645, https://doi.org/10.1016/J.JWEIA.2021.104645.

[27] Z.T. Ai, C.M. Mak, Large eddy simulation of wind-induced interunit dispersion around multistory buildings, Indoor Air 26 (2) (Apr. 2016) 259–273, https://doi.org/10.1111/ina.12200.

[28] J. Leng, Q. Wang, K. Liu, Sustainable design of courtyard environment: from the perspectives of airborne diseases control and human health, Sustain. Cities Soc. 62 (Nov. 2020), 102405, https://doi.org/10.1016/J.SCS.2020.102405.

[29] X. Liu, X. Lv, Z. Peng, C. Shi, Experimental study of airflow and pollutant dispersion in cross-ventilated multi-room buildings: effects of source location and ventilation path, Sustain. Cities Soc. 52 (Jan. 2020), 101822, https://doi.org/10.1016/J.SCS.2019.101822.

[30] S.M. Salim, S.C. Cheah, A. Chan, Numerical simulation of dispersion in urban street canyons with avenue-like tree plantings: comparison between RANS and LES, Build. Environ. 46 (9) (Sep. 2011) 1735–1746, https://doi.org/10.1016/J.BUILDENV.2011.01.032.

[31] A.W.M. Yazid, N.A.C. Sidik, S.M. Salim, K.M. Saqr, A review on the flow structure and pollutant dispersion in urban street canyons for urban planning strategies, Simulation 90 (8) (Aug. 2014) 892–916, https://doi.org/10.1177/0037549714528046.

[32] S. Janhäll, Atmospheric environment, Review on urban vegetation and particle air pollution - Deposition and dispersion 105 (Mar. 01, 2015) 130–137, https://doi.org/10.1016/j.atmosenv.2015.01.052. Elsevier Ltd.

[33] X.-B. Li, et al., The impacts of roadside vegetation barriers on the dispersion of gaseous traffic pollution in urban street canyons, Urban For. Urban Green. 17 (Jun. 2016) 80–91, https://doi.org/10.1016/j.ufug.2016.03.006.

[34] Y. Zhang, Z. Gu, C.W. Yu, Impact factors on airflow and pollutant dispersion in urban street canyons and comprehensive simulations: a review, Current Pollution Reports 6 (4) (Dec. 2020) 425–439, https://doi.org/10.1007/s40726-020-00166-0. Springer Science and Business Media Deutschland GmbH.

[35] C. Yuan, E. Ng, L.K. Norford, Improving air quality in high-density cities by understanding the relationship between air pollutant dispersion and urban morphologies, Build. Environ. 71 (Jan. 2014) 245–258, https://doi.org/10.1016/J.BUILDENV.2013.10.008.

[36] M. Lateb, R.N. Meroney, M. Yataghene, H. Fellouah, F. Saleh, M.C. Boufadel, On the use of numerical modelling for near-field pollutant dispersion in urban environments - a review, Environ. Pollut. 208 (Jan. 2016) 271–283, https://doi.org/10.1016/j.envpol.2015.07.039.

[37] Y. Zhao, C. Jiang, X. Song, Numerical evaluation of turbulence induced by wind and traffic, and its impact on pollutant dispersion in street canyons, Sustain. Cities Soc. 74 (Nov. 2021), 103142, https://doi.org/10.1016/J.SCS.2021.103142.

[38] A.M. Hassan, A.A. Elmokadem, N.A. Megahed, O.M. Abo Eleinen, Urban morphology as a passive strategy in promoting outdoor air quality, J. Build. Eng. 29 (May 2020) 101204, https://doi.org/10.1016/J.JOBE.2020.101204.

[39] X. Guo, M. Zhang, Z. Gao, J. Zhang, R. Buccolieri, Neighborhood-scale dispersion of traffic-related PM2.5: simulations of nine typical residential cases from Nanjing, Sustain. Cities Soc. 90 (Mar. 2023), 104393, https://doi.org/10.1016/J.SCS.2023.104393.

[40] L. He, J. Hang, X. Wang, B. Lin, X. Li, G. Lan, Numerical investigations of flow and passive pollutant exposure in high-rise deep street canyons with various street aspect ratios and viaduct settings, Sci. Total Environ. 584 (585) (Apr. 2017) 189–206, https://doi.org/10.1016/j.scitotenv.2017.01.138.

[41] F. Yang, Y. Kang, Y. Gao, K. Zhong, Numerical simulations of the effect of outdoor pollutants on indoor air quality of buildings next to a street canyon, Build. Environ. 87 (May 2015) 10–22, https://doi.org/10.1016/j.buildenv.2015.01.008.

[42] J. Hang, M. Lin, D.C. Wong, X. Wang, B. Wang, R. Buccolieri, On the influence of viaduct and ground heating on pollutant dispersion in 2D street canyons and toward single-sided ventilated buildings, Atmos. Pollut. Res. 7 (5) (Sep. 2016) 817–832, https://doi.org/10.1016/J.APR.2016.04.009.

[43] Y. Hu, et al., Impact of indoor-outdoor temperature difference on building ventilation and pollutant dispersion within urban communities, Atmosphere 13 (1) (2022) 28, https://doi.org/10.3390/ATMOS13010028. Dec. 2021.

[44] J.L. Santiago, et al., Indoor-outdoor pollutant concentration modelling: a comprehensive urban air quality and exposure assessment, Air Qual Atmos Health (May 2022) 1–26, https://doi.org/10.1007/S11869-022-01204-0/FIGURES/17.

[45] Y. Dai, C.M. Mak, Y. Zhang, D. Cui, J. Hang, Investigation of interunit dispersion in 2D street canyons: a scaled outdoor experiment, Build. Environ. 171 (Mar. 2020), 106673, https://doi.org/10.1016/J.BUILDENV.2020.106673.

[46] Y. Dai, C.M. Mak, J. Hang, F. Zhang, H. Ling, Scaled outdoor experimental analysis of ventilation and interunit dispersion with wind and buoyancy effects in street canyons, Energy Build. 255 (Jan. 2022), 111688, https://doi.org/10.1016/J.ENBUILD.2021.111688.

[47] P.Y. Cui, et al., Wind-tunnel measurements and LES simulations of air pollutant dispersion caused by fire-induced buoyancy plume inside two parallel street canyons, Process Saf. Environ. Protect. 140 (Aug. 2020) 151–169, https://doi.org/10.1016/J.PSEP.2020.04.047.

[48] K. Zheng, P. Ortner, Y.W. Lim, T.J. Zhi, Ventilation in worker dormitories and its impact on the spread of respiratory droplets, Sustain. Cities Soc. 75 (Dec. 2021), 103327, https://doi.org/10.1016/J.SCS.2021.103327.

[49] Y. Xiong, H. Chen, Impacts of uneven surface heating of an ideal street canyon on airflows and indoor ventilation: numerical study using OpenFOAM coupled with EnergyPlus, Build. Simulat. 15 (2022) 265–280, https://doi.org/10.1007/s12273-021-0788-5.

[50] X. Yang, et al., Integrated assessment of indoor and outdoor ventilation in street canyons with naturally-ventilated buildings by various ventilation indexes, Build. Environ. 169 (Feb. 2020), 106528, https://doi.org/10.1016/j.buildenv.2019.106528.

[51] Z.T. Ai, C.M. Mak, J.L. Niu, Numerical investigation of wind-induced airflow and interunit dispersion characteristics in multistory residential buildings, Indoor Air 23 (5) (Oct. 2013) 417–429, https://doi.org/10.1111/ina.12041.

[52] Z. Tong, Y. Chen, A. Malkawi, G. Adamkiewicz, J.D. Spengler, Quantifying the impact of traffic-related air pollution on the indoor air quality of a naturally ventilated building, Environ. Int. 89 (90) (Apr. 2016) 138–146, https://doi.org/10.1016/j.envint.2016.01.016.

[53] D. Cui, C. Mak, J. Niu, Effect of balconies and upper–lower vents on ventilation and indoor air quality in a wind-induced, naturally ventilated building, Build. Serv. Eng. Res. Tecnol. 35 (4) (Jul. 2014) 393–407, https://doi.org/10.1177/0143624413499353.

[54] J. Hang, R. Buccolieri, X. Yang, H. Yang, F. Quarta, B. Wang, Impact of indoor-outdoor temperature differences on dispersion of gaseous pollutant and particles in idealized street canyons with and without viaduct settings, Build. Simulat. 12 (2018) 285–297, https://doi.org/10.1007/s12273-018-0476-2.

[55] Y.W. Dai, C.M. Mak, Z.T. Ai, 2, Computational Fluid Dynamics Simulation of Wind-Driven Inter-unit Dispersion Around Multi-Storey Buildings: Upstream Building Effect, vol. 28, Dec. 2017, pp. 217–234, https://doi.org/10.1177/1420326X17745943, 10.1177/1420326X17745943.

[56] J. Wang, Q. Huo, T. Zhang, S. Wang, F. Battaglia, Numerical investigation of gaseous pollutant cross-transmission for single-sided natural ventilation driven by buoyancy and wind, Build. Environ. 172 (Apr. 2020), 106705, https://doi.org/10.1016/j.buildenv.2020.106705.

[57] Y. Jiang, D. Alexander, H. Jenkins, R. Arthur, Q. Chen, Natural ventilation in buildings: measurement in a wind tunnel and numerical simulation with large-eddy simulation, J. Wind Eng. Ind. Aerod. 91 (3) (Feb. 2003) 331–353, https://doi.org/10.1016/S0167-6105(02)00380-X.

[58] Y. Wu, J. Niu, Assessment of mechanical exhaust in preventing vertical cross-household infections associated with single-sided ventilation, Build. Environ. 105 (Aug. 2016) 307–316, https://doi.org/10.1016/j.buildenv.2016.06.005.

[59] M. Perino, P. Heiselberg, Short-term airing by natural ventilation - modeling and control strategies, Indoor Air 19 (5) (Feb. 2009) 357–380, https://doi.org/10.1111/J.1600-0668.2009.00597.X.

[60] Z.T. Ai, C.M. Mak, Wind-induced single-sided natural ventilation in buildings near a long street canyon: CFD evaluation of street configuration and envelope design, J. Wind Eng. Ind. Aerod. 172 (Jan. 2018) 96–106, https://doi.org/10.1016/J.JWEIA.2017.10.024.

[61] E. Dascalaki, et al., On the combination of air velocity and flow measurements in single sided natural ventilation configurations, Energy Build. 24 (2) (Jul. 1996) 155–165, https://doi.org/10.1016/0378-7788(96)00973-5.

[62] C. Gromke, R. Buccolieri, S. Di Sabatino, B. Ruck, Dispersion study in a street canyon with tree planting by means of wind tunnel and numerical investigations - evaluation of CFD data with experimental data, Atmos. Environ. 42 (37) (Dec. 2008) 8640–8650, https://doi.org/10.1016/j.atmosenv.2008.08.019.

[63] Karlsruhe Institute of Technology, "CODASC, Concentration Data of Street Canyons, Laboratory of Building- and Environmental Aerodynamics, 2008, 2008, https://www.windforschung.de/CODASC.htm. (Accessed 13 October 2020).

[64] Environmental Meteorology - Prognostic Microscale Wind Field Models - Evaluation for Flow Around Buildings and Obstacles, 2017. Jan. 27, 2023, https://www.beuth.de/en/technical-rule/vdi-3783-blatt-9/267500591.

[65] J. Franke, et al., Recommendations on the use of CFD in wind engineering, in: Proceedings of the International Conference on Urban Wind Engineering and Building Aerodynamics, 2004. C.1.1–C1.11.

[66] S.M. Salim, R. Buccolieri, A. Chan, S. Di Sabatino, Numerical simulation of atmospheric pollutant dispersion in an urban street canyon: comparison between RANS and LES, J. Wind Eng. Ind. Aerod. 99 (2) (Feb. 2011) 103–113, https://doi.org/10.1016/j.jweia.2010.12.002.

[67] Y. Wu, T.C.W. Tung, J. Niu, Experimental analysis of driving forces and impact factors of horizontal inter-unit airborne dispersion in a residential building, Build. Environ. 151 (Mar. 2019) 88–96, https://doi.org/10.1016/J.BUILDENV.2019.01.028.

[68] Ansys®, Ansys 18.2 (documentation), Ansys, https://www.sharcnet.ca/Software/Ansys/18.2.2/en-us/help/flu_th/flu_th_sec_turb_near_wall_overview.html.

[69] B. Blocken, Computational Fluid Dynamics for urban physics: importance, scales, possibilities, limitations and ten tips and tricks towards accurate and reliable simulations, Build. Environ. 91 (Sep. 2015) 219–245, https://doi.org/10.1016/j.buildenv.2015.02.015.

[70] Y. dong Huang, M. zhen Li, S. qi Ren, M. jie Wang, P. yi Cui, Impacts of tree-planting pattern and trunk height on the airflow and pollutant dispersion inside a street canyon, Build. Environ. 165 (Nov. 2019), https://doi.org/10.1016/J.BUILDENV.2019.106385.

[71] S.J. Mei, Z. Luo, F.Y. Zhao, H.Q. Wang, Street canyon ventilation and airborne pollutant dispersion: 2-D versus 3-D CFD simulations, Sustain. Cities Soc. 50 (Oct. 2019), 101700, https://doi.org/10.1016/j.scs.2019.101700.

[72] L. Zhang, Z. Zhang, S. McNulty, P. Wang, The mitigation strategy of automobile generated fine particle pollutants by applying vegetation configuration in a street-canyon, J. Clean. Prod. 274 (Nov. 2020), 122941, https://doi.org/10.1016/J.JCLEPRO.2020.122941.

[73] V.A. Karkoulias, P.E. Marazioti, D.P. Georgiou, E.A. Maraziotis, Computational Fluid Dynamics modeling of the trace elements dispersion and comparison with measurements in a street canyon with balconies in the city of Patras, Greece, Atmos. Environ. 223 (Feb. 2020), 117210, https://doi.org/10.1016/J.ATMOSENV.2019.117210.

[74] J.L. Santiago, et al., Performance evaluation of a multiscale modelling system applied to particulate matter dispersion in a real traffic hot spot in Madrid (Spain), Atmos. Pollut. Res. 11 (1) (Jan. 2020) 141–155, https://doi.org/10.1016/J.APR.2019.10.001.

[75] B. Sanchez, et al., Modelling NOX concentrations through CFD-RANS in an urban hot-spot using high resolution traffic emissions and meteorology from a mesoscale model, Atmos. Environ. 163 (Aug. 2017) 155–165, https://doi.org/10.1016/J.ATMOSENV.2017.05.022.

[76] B. Blocken, T. Stathopoulos, P. Saathoff, X. Wang, Numerical evaluation of pollutant dispersion in the built environment: comparisons between models and experiments, J. Wind Eng. Ind. Aerod. 96 (10–11) (Oct. 2008) 1817–1831, https://doi.org/10.1016/J.JWEIA.2008.02.049.

[77] VDI 3783 Blatt 12 - environmental meteorology - physical modelling of flow and dispersion processes in the atmospheric boundary layer - application of wind tunnels, in: https://www.vdi.de/en/home/vdi-standards/details/vdi-3783-blatt-12-environmental-meteorology-physical-modelling-of-flow-and-dispersion-processes-in-the-atmospheric-boundary-layer-application-of-wind-tunnels. (Accessed 10 July 2023).

[78] Z. Tan, M. Tan, X. Sui, C. Jiang, H. Song, Impact of source shape on pollutant dispersion in a street canyon in different thermal stabilities, Atmos. Pollut. Res. 10 (6) (Nov. 2019) 1985–1993, https://doi.org/10.1016/J.APR.2019.09.005.

[79] C.H. Liu, C.T. Ng, C.C.C. Wong, A theory of ventilation estimate over hypothetical urban areas, J. Hazard Mater. 296 (Oct. 2015) 9–16, https://doi.org/10.1016/J.JHAZMAT.2015.04.018.

[80] Y. Dai, C.M. Mak, Z. Ai, J. Hang, Evaluation of computational and physical parameters influencing CFD simulations of pollutant dispersion in building arrays, Build. Environ. 137 (Jun. 2018) 90–107, https://doi.org/10.1016/J.BUILDENV.2018.04.005.

[81] M. Lateb, C. Masson, T. Stathopoulos, C. Bédard, Effect of stack height and exhaust velocity on pollutant dispersion in the wake of a building, Atmos. Environ. 45 (29) (Sep. 2011) 5150–5163, https://doi.org/10.1016/J.ATMOSENV.2011.06.040.

[82] S. Murakami, Overview of turbulence models applied in CWE–1997, J. Wind Eng. Ind. Aerod. 74 (76) (Apr. 1998) 1–24, https://doi.org/10.1016/S0167-6105(98)00004-X.

[83] R. Britter, et al., MODEL EVALUATION GUIDANCE and PROTOCOL DOCUMENT COST Action 732 QUALITY ASSURANCE and IMPROVEMENT of MICRO-SCALE METEOROLOGICAL MODELS as: Title of the Book and Action Number, 2007.

[84] R. Meroney, R. Ohba, B. Leitl, H. Kondo, D. Grawe, and Y. Tominaga, "Review of CFD Guidelines for Dispersion Modeling", doi: 10.3390/fluids1020014.

[85] C. Li, L. Liu, W. Tan, Evaluation of RSM for simulating dispersion of CO2 cloud in flat and urban terrains, Aerosol Air Qual. Res. 19 (2) (Feb. 2019) 390–398, https://doi.org/10.4209/AAQR.2018.09.0328.

[86] R.N. Meroney, B.M. Leitl, S. Rafailidis, M. Schatzmann, Wind-tunnel and numerical modeling of flow and dispersion about several building shapes, J. Wind Eng. Ind. Aerod. 81 (1–3) (May 1999) 333–345, https://doi.org/10.1016/S0167-6105(99)00028-8.

[87] J.C. Chang, S.R. Hanna, Air quality model performance evaluation, Meteorol. Atmos. Phys. 87 (1) (Jun. 2004) 167–196, https://doi.org/10.1007/S00703-003-0070-7, 2004 87:1.

[88] M. Liu, C. Jimenez-Bescos, J. Calautit, CFD investigation of a natural ventilation wind tower system with solid tube banks heat recovery for mild-cold climate, J. Build. Eng. 45 (2022), 103570, https://doi.org/10.1016/j.jobe.2021.103570.

[89] P. Nejat, J.K. Calautit, Y. r Fekri, M. Sheikhshahrokhdehkordi, H. Alsaad, C. Voelker, Influence of terrain and atmospheric boundary layer on the ventilation and thermal comfort performance of windcatchers, J. Build. Eng. 73 (2023), 106791, https://doi.org/10.1016/j.jobe.2023.106791.

[90] M. Liu, C. Jimenez-Bescos, J.K. Calautit, Performance evaluation of wind tower natural ventilation with passive solid tube heat recovery based on CO2 levels, J. Build. Eng. 72 (2023), 106457, https://doi.org/10.1016/j.jobe.2023.106457.

[91] M. Bady, S. Kato, H. Huang, Towards the application of indoor ventilation efficiency indices to evaluate the air quality of urban areas, Build. Environ. 43 (12) (Dec. 2008) 1991–2004, https://doi.org/10.1016/J.BUILDENV.2007.11.013.

[92] D. L, O. E, Calculation of age and local purging flow rate in rooms, Mar. 26, 2023, https://www.aivc.org/resource/calculation-age-and-local-purging-flow-rate-rooms-0, 1987.

[93] Z.T. Ai, C.M. Mak, From street canyon microclimate to indoor environmental quality in naturally ventilated urban buildings: issues and possibilities for improvement, Build. Environ. 94 (Dec. 2015) 489–503, https://doi.org/10.1016/j.buildenv.2015.10.008.

[94] C. Gromke, B. Ruck, On the impact of trees on dispersion processes of traffic emissions in street canyons, Boundary-Layer Meteorol. 131 (2009) 19–34, https://doi.org/10.1007/s10546-008-9301-2.

[95] I.B. Celik, U. Ghia, P.J. Roache, C.J. Freitas, H. Coleman, P.E. Raad, Procedure for estimation and reporting of uncertainty due to discretization in CFD applications, Journal of Fluids Engineering, Transactions of the ASME 130 (7) (Jul. 2008) 780011–780014, https://doi.org/10.1115/1.2960953/444689.